Università degli Studi di Milano - Bicocca

FACOLTÀ DI SCIENZE MATEMATICHE, FISICHE E NATURALI
Corso di Laurea Magistrale in Fisica

Measuring the lifetime of muons with plastic scinillators

Autori:
Tiziano Bevilacqua
Federica Colombina
Alessandro Tarabini
Enrico Tarabini

Anno Accademico 2018-2019

Contents

Chapter 1

Introduction

1.1 Aim of the experiment

The aim of the experiment is to measure the mean lifetime of cosmic-ray muons in plastic scintillators; there are two possible decay modes:

$$\mu^- \to e^- + \bar{\nu}_e + \nu_\mu, \qquad \mu^+ \to e^+ + \nu_e + \bar{\nu}_\mu \tag{1.1}$$

which means the electron (or positron) is the only detectable particle in the final state. Plastic scintillators are used due to their physical properties: their short response time makes them suitable for temporal measurements and the surface is large enough to detect a significant amount of cosmic rays.

1.2 Cosmic rays

Cosmic rays are originated outside the atmosphere and are subdivided in two categories:

- Primary cosmic rays, mainly composed of protons and alpha particles (97%); they come from astrophysical sources, such as supernovae and black holes.
- Secondary cosmic rays, produced from the interactions of primary cosmic rays with Earth's atmosphere.

The energy spectrum of cosmic rays (Fig. 1.1a) covers 12 orders of magnitude on the energy scale and 32 orders of magnitude on the flux scale. The strong interaction of protons from primary cosmic rays with air nuclei produces pions, K mesons and, more rarely, other hadrons; these particles are unstable and their decay products, such as muons and neutrinos, can be detected on Earth. This process is sketched in Figure 1.1b.

The muon lifetime is approximately equal to 2 μs, much larger than that of pions and kaons, which means secondary cosmic rays become richer and richer in muons as they go deeper in the atmosphere.

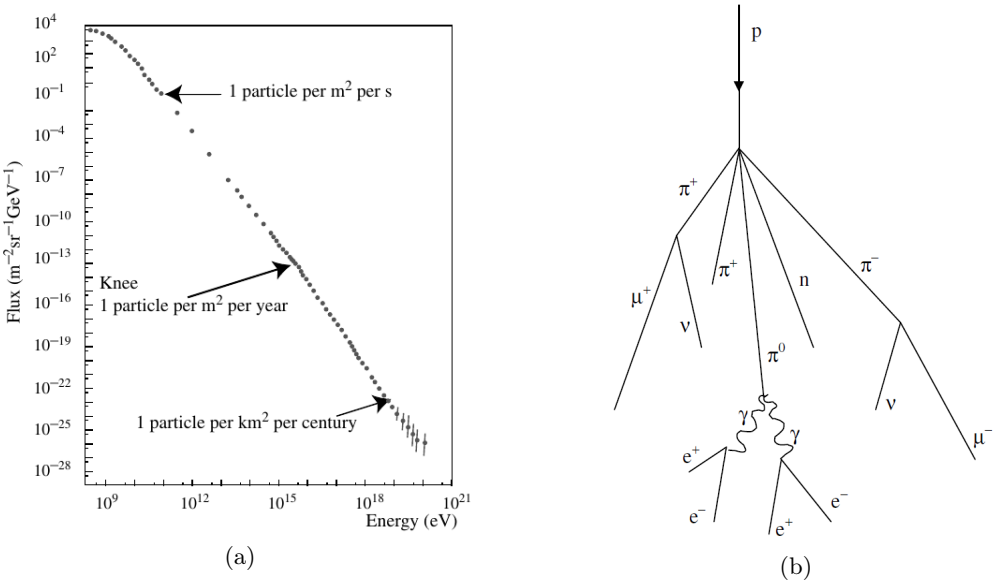

Figure 1.1: *(a) The cosmic ray flux. (b) Secondary cosmic ray production.*

1.3 Interaction of muons with matter

The interactions displayed by muons are mainly due to collisions with atomic electrons during their passage through matter, producing atomic ionisation or excitation and radiative emissions. The way in which muons interact with matter strongly depends on their energies; ionisation is the dominant process between a few Mev and dozen of Gev. The average energy loss in this interval can be described with the Bethe-Bloch formula:

$$-\frac{dE}{dx} = 4\pi r_e^2 m_e c^2 N_A \frac{Z}{A}\frac{1}{\beta^2}\rho\left[\ln\frac{2m_e v^2\gamma^2}{I} - \beta^2\right] \tag{1.2}$$

where r_e and m_e are the electron classic radius and its mass, while Z, ρ and A refer to the absorber material and v is the velocity of muons. The shape of this function shows important differences in different media, as shown in Figure 1.2: all the curves decrease rapidly at small momenta (roughly as $1/\beta^2$), reach a minimum for $\beta\gamma \simeq 3-4$ and then increase very slowly.

The Bethe-Bloch formula is only valid in the interval corresponding to $0.05 < \beta\gamma < 500$; at lower momenta, a large fraction of the energy loss is due to the excitation of atomic and molecular levels, since the particle speed is comparable to the speed of the atomic electrons. At larger energies, the bremsstrahlung losses in the nuclear fields become more important than ionisation; this happens at a few hundred GeV for pions and muons, while much larger energies are needed for protons.

The *critical energy* is defined as the energy at which the ionisation and radiative loss

rates are equal. For muons and pions in materials such as carbon, this occurs at several hundred GeV. The energy of cosmic-ray muons is 2-3 order of magnitude smaller than this critical energy, which means ionisation is the main cause of energy loss in plastic scintillators.

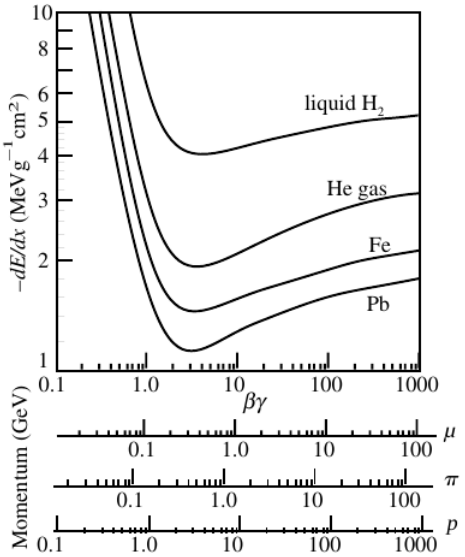

Figure 1.2: *Bethe-Bloch formula for relativistic particles of unit charge.*

1.4 Lifetimes of positive and negative muons in matter

Muons show different behaviors when they are stopped in matter, depending on their charge. Positive muons μ^+ have a repulsive interaction with atomic nuclei, which means their lifetime is similar to that of free muons (approximately equal to 2,2 μs). On the contrary, negative muons μ^- feel the coulombic attraction that comes from the nuclei and can be absorbed by the atom. The captured muon falls down to the ground state, causing the emission of Auger electrons or characteristic electromagnetic radiation, and eventually disappears either by decaying or by being captured from the nucleus via the weak interaction:

$$\mu^- + p \rightarrow n + \nu_\mu \tag{1.3}$$

The total capture rate depends on the atomic number Z of the absorber material: as its value increases, the radius of the atomic orbital becomes smaller and the muon can be captured with higher probability, since it's closer to the nucleus. The amplitude is described by the Primakoff formula:

$$\Gamma_{capture} = Z_{eff}^4 X_1 \left[1 - X_2 \left(\frac{A-Z}{2A}\right)\right] \tag{1.4}$$

where X_1 is the probability of nuclear capture by the hydrogen atom, X_2 is a correction due to the Pauli exclusion principle and Z_{eff} is the effective nuclear charge. Alternatively, as mentioned before, the muon can decay when it's in a bound state with the nucleus; in this case the decay amplitude becomes equal to

$$\Gamma_{bound} = Q\Gamma_{free} \tag{1.5}$$

where Q is the Huff factor, which is a small correction (always ≤ 1) taking into account the fact that the decay rate is reduced for a bound μ^-: the binding energy reduces the total amount of energy avaiable. The total decay amplitude is then:

$$\Gamma_{tot} = \Gamma_{capture} + \Gamma_{bound} \tag{1.6}$$

whose inverse gives the lifetime of negative muons.
For our experiment, we are interested in lifetimes in carbon that are: $\tau_{\mu^+} = 2197ns$ and $\tau_{\mu^-} = 2026ns$.

Chapter 2

Experimental apparatus

2.1 Equipment

2.1.1 Scintillators

Scintillators are able to detect ionizing radiation from the scintillation light produced in certain materials: the energy deposition causes atomic or molecular excitation in the detectors and the process of de-excitation leads to the emission of light. These detectors must be coupled to an electronic light sensor such as a photomultiplier tube, in order to convert the light output into a corresponding electrical signal.

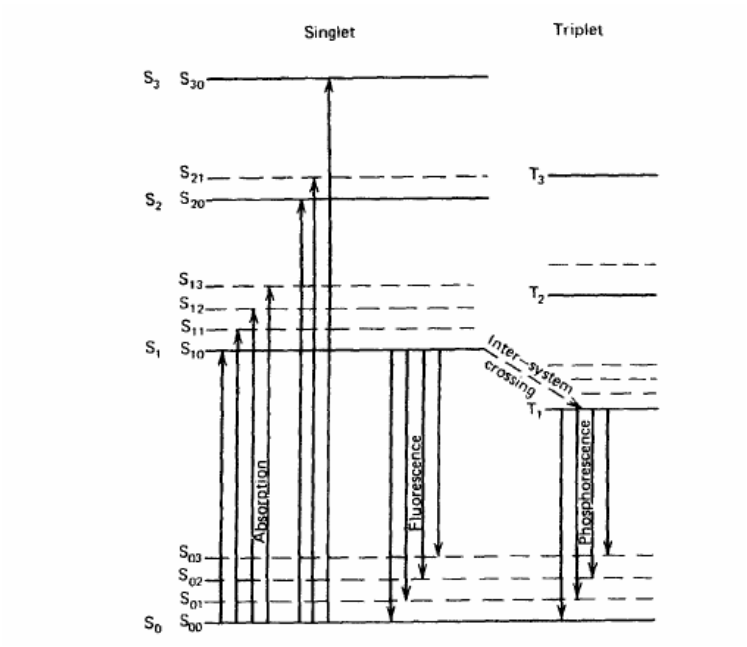

Figure 2.1: *Energy levels of an organic molecule with absorption and emission processes.*

This experiment involves the use of organic scintillators, which are characterized by a low Z and a density ρ of $\sim$ 1g/cm^3. Their time response is relatively fast (about 2-3 ns), making them suitable for time measurements; scintillation light comes from transitions in the energy level structure of a single molecule, as shown in Figure 2.1: the emission of light always starts from the lowest vibrational state of the singlet state S_1. Furthermore, the process of atomic de-excitation doesn't always lead to S_{00}, which is the lowest vibrational level in the ground state: this explains why usually organic scintillators can be transparent to their own fluorescence emission.
Five scintillators have been used in total, their characteristics are listed in Table 2.1. Caracalla, the smallest and the better one, was used just to characterize the others. Nerone and Domiziano work with a light guide and a photomultiplier, instead Tito and Vespasiano use an optical fiber system to collect light and have a smaller active region.

Table 2.1: *List of the scintillators used in the experiment with related dimensions. Only the active zones of the detectors are considered.*

Scintillator name	length × width × height [cm]
Nerone	80 × 30 × 1
Tito	42 × 26 × 1.5
Vespasiano	42 × 26 × 1.5
Domiziano	80 × 30 × 1
Caracalla	27 × 8 × 1

2.1.2 Electronic instrumentation

The electronic instrumentation used during the whole experiment is listed below:

- 12 Slot NIM Crate, mod NIM 8304 (C.A.E.N.)
- Quad Scaler And Preset Counter/Timer N1145 (CAEN)
- Programmable logic unit 81A (CAEN)
- NIM Model 622C Quad 2-Fold Logic Unit (LeCroy)
- 8 Channel Discriminator 96 (CAEN)
- High Voltage Power Supply NHQ 214M (ISEG)
- High Voltage Power Supply N1470AL (CAEN)
- Dual timer 2255B (CAEN)
- 4-8 Logic FAN-IN/FAN-OUT N454 (CAEN)

- Delay N9053
- Desktop Digitizer DT5751 (CAEN)

2.2 Scintillator characterization

This first part of the experiment aims to find the optimal working conditions for each scintillator, focusing on the supply voltage of the photomultiplier tube and the discriminator threshold.

2.2.1 Plateau curves

Outputs generated by muons should be distinguished from their vast background. Once a supply voltage value has been set, the signal coming from scintillators is sent to one of the discriminator inputs, which gives a logic signal if the linear input is above the threshold that has been set. Events occurring in a 45-seconds interval are counted and the measure is repeated for different threshold values; the resulting graphs are shown in Figure 2.2.

When the threshold is low, counts are high due to the natural radioactivity background. As the threshold is raised, the counts reduce since the discriminator stops more and more background events. The decrease in counting continues until a plateau-shaped region is reached. This region corresponds to the optimal working condition: all the background is stopped by the discriminator and we only count muons. Going further in the growth of the threshold results again in a reduction in counting since also muon events are stopped by the discriminator. The whole process is then repeated for different supply voltage values; the curve having the largest plateau should correspond to the optimal voltage for that scintillator.

The flux of muons at sea level is about $1\frac{muon}{cm^2\ min}$. Knowing the area of the scintillators (Table 2.1) and the time interval (45 seconds), it is possible to make a prediction about the expected number of events in the plateau region.

- Caracalla $\rightarrow\sim$160 muons
- Nerone and Domiziano $\rightarrow\sim$1800 muons
- Tito and Vespasiano $\rightarrow\sim$820 muons

The measured plateau of Caracalla is in agreement with the expectation, proving its good quality. Tito does not show a clear plateau, even though in the red curve in Figure 2.2 there is a semblance of a plateau near the expectation. The measured plateaus of Nerone, Domiziano and Vespasiano are not as the expected ones. This can be caused by the noise that affect their waveform.
It should be noted that we measured the plateau of Nerone and Domiziano at different

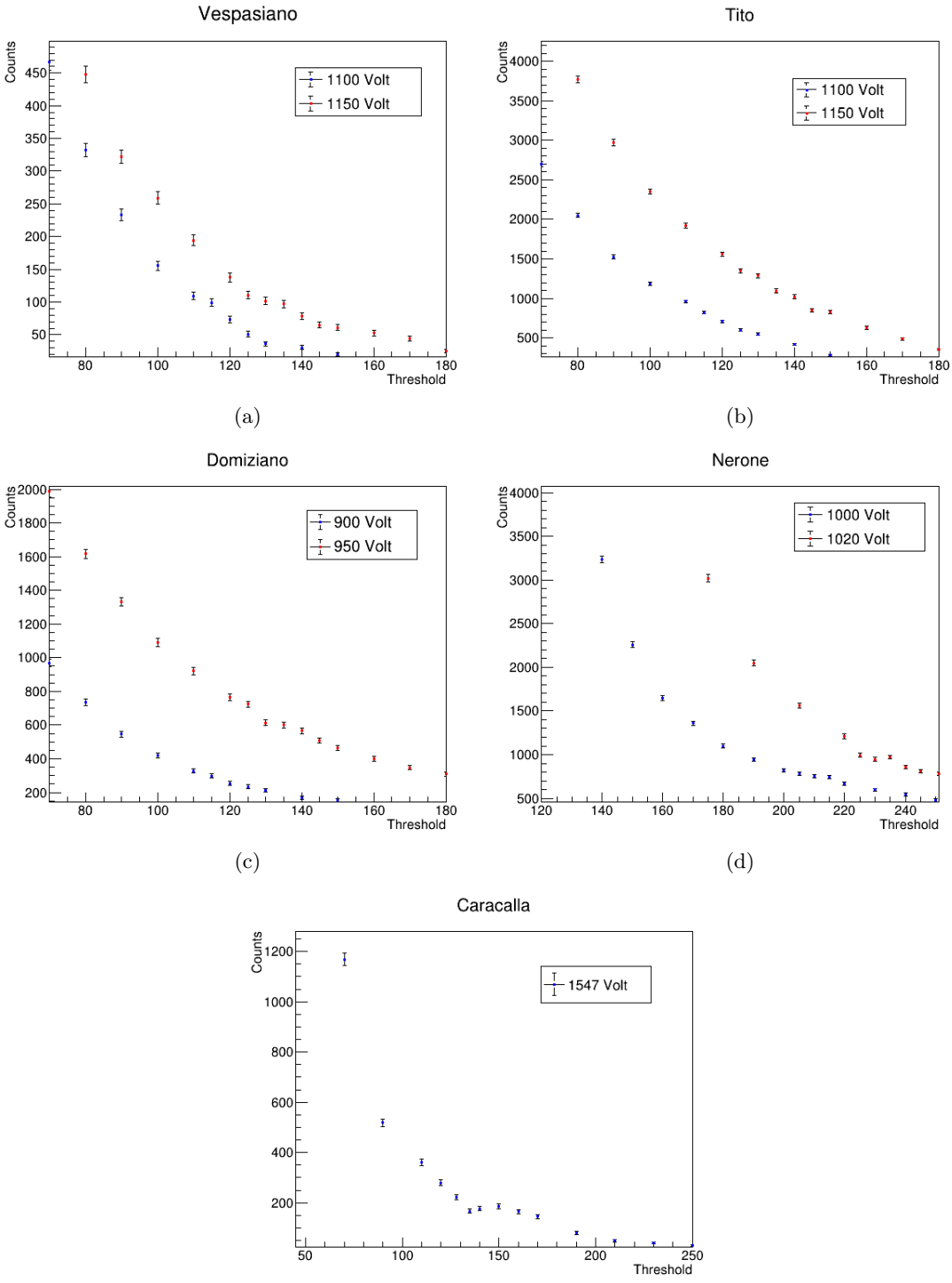

Figure 2.2: *(a) Vespasiano, (b) Tito, (c) Domiziano, (d) Nerone and (e) Caracalla.*

HV levels, even though *a priori* they should be chosen equal. This choice was due to the better waveform of Domiziano at lower supply voltage. Only Nerone, Domiziano, Caracalla and Tito will be considered from now on, Vespasiano will not be used due to geometric factors and the poor quality of its signal (see Figure 2.3).

Figure 2.3: *An example of lost event due to geometric factor: the muon stops in the second scintillator and subsequently decays; the electron, which is the only detectable particle among the decay products, is not detected by the first scintillator.*

2.2.2 Efficiency

The working point (combination of high voltage and threshold values) of each scintillator is found by optimizing their efficiencies. To perform such measurement, the electronic chain is like the one in Figure 2.4: the first and the third scintillator are set with a reasonable HV (the values chosen in the previous section, while measuring the plateau), and a threshold which lies in the middle of their plateaus, though ours are really narrow and not sharp.

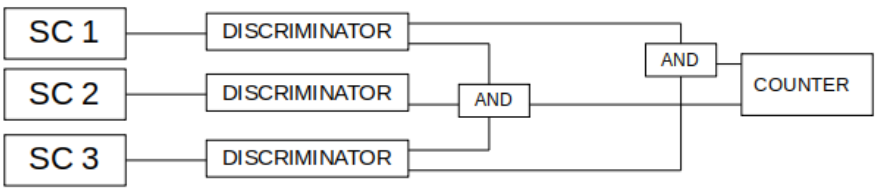

Figure 2.4: *Electronic chain for the efficiency measure*

The efficiency of the middle scintillator will be given by the ratio of triple events (coincidence of an event in all the scintillators) and double events (coincidence in SC1

and SC3). Indeed, if ε_i is the efficiency of the ith scintillator:

$$N_{double} = N\varepsilon_1\varepsilon_3 \tag{2.1}$$

$$N_{triple} = N\varepsilon_1\varepsilon_2\varepsilon_3 \tag{2.2}$$

$$\varepsilon_2 = \frac{N_{triple}}{N_{double}} \tag{2.3}$$

The error of the efficiency is calculated considering that the measurement of the efficiency is equal to do N_{double} trials for which each trial has a success probability ϵ and N_{triple} is the number of success.

$$\sigma_{Ntriple} = \sqrt{N_{double}\epsilon(1-\varepsilon)} \tag{2.4}$$

$$\sigma_\varepsilon = \frac{\sigma_{Ntriple}}{N_{double}} = \sqrt{\frac{\varepsilon(1-\varepsilon)}{N_{double}}} \tag{2.5}$$

The efficiency of a certain scintillator is independent from the other two efficiencies but it is affected by geometrical effects. To reduced them, we tried to modify the relative positions of the scintillators in many arrangements, an example is reported in Figure 2.5. But these configurations just partially solve our problem, so we decided to use Caracalla as bottom scintillator.

The results are shown in Figure 2.6, 2.7 and 2.8 (full data can be read in Appendix B).
The results show that efficiencies have a plateau (ε between 90% and 100%) where the efficiency is at its maximum, but when the threshold reach a certain value the number of triple events start dropping and so does the efficiency.
Optimizing the efficiency means setting the threshold and the HV to have a large plateau to guarantee stability, and to have a high efficiency to reduce losses of events. Our final choices are reported in Table 2.2.
To put our apparatus in such configuration it is necessary to reduce the thresholds and move them away from the muon plateau. This can cause an accidental triple event due to a no-muon event. However, the probability of having casual coincidence of a background event during a coincidence gate ΔT is:

$$P = 1 - \exp\left(-\Delta r \cdot \Delta T\right) \tag{2.6}$$

with Δr is the difference between the rate at the point where the threshold is set and the plateau rate. The values of this probability for the three scintillator are about $10^{-4} \div 10^{-6}$, so it is negligible.

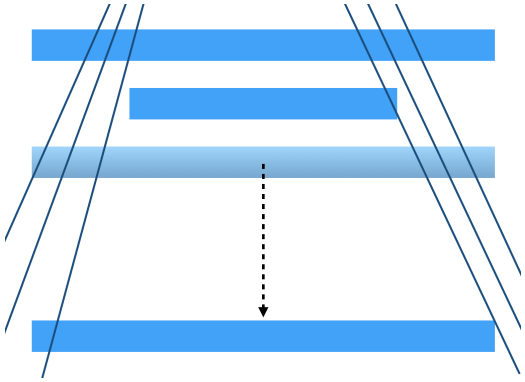

Figure 2.5: *Widening the distance between the upper two detectors and the lower one improves but not solves the problem arose by geometric effects. While reducing the geometric effect some fake doubles still appear and a few real events are not detected anymore.*

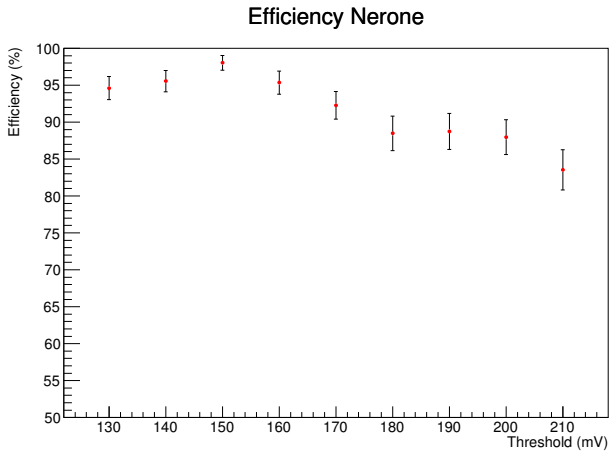

Figure 2.6: *HV: Nerone 1000V, Domiziano 1000V, Caracalla 1550 V. Thresholds: Domiziano 210 mV, Caracalla 150 mV. As working point a threshold of 150 mV and a 1000V HV have been chosen.*

Table 2.2: *Working points and efficiencies of Nerone, Tito and Domiziano*

Scintillator	Threshold	HV	Efficiency	Error
Nerone	150 mV	1000 V	98.0%	1.0
Tito	50 mV	1200 V	87.9%	1.7
Domiziano	110 mV	1000 V	98.4%	0.7

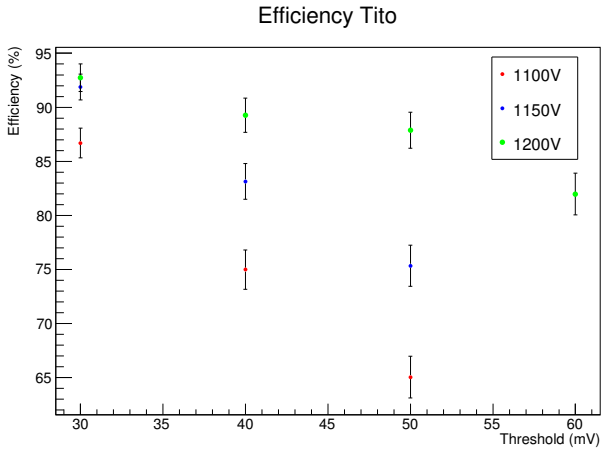

Figure 2.7: *HV: Nerone 1000V, Caracalla 1550 V. Thresholds: Domiziano 210 mV, Caracalla 150 mV. As working point a threshold of 50 mV and a 1200V HV have been chosen.*

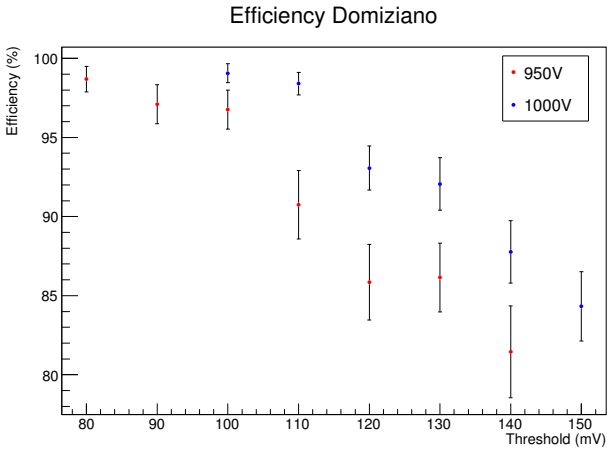

Figure 2.8: *HV: Nerone 1000V, Caracalla 1550 V. Thresholds: Nerone 210 mV, Caracalla 150 mV. As working point a threshold of 110 mV and a 1000V HV have been chosen.*

2.2.3 Uniformity

Since our scintillators are not well-functioning, it is useful to study the uniformity of the efficiency along all their area. The setup is the same as the previous one, but rather than keeping Caracalla fixed in the centre position, it is moved from one end to the other. Actually, this test was made before the final choice about the thresholds and HVs to use for our experiment. The ones used for this test are slightly different from the values reported in Table 2.2. Since our aim is just to verify the intrinsic uniformity of the scintillators, and since the values are not too different from the chosen ones, we did not find necessary to redo the test with the final combination of threshold and HVs and take as valid these results.

The results are displayed graphically as reported in Table 2.3: the position of the column represents the position of the tested area; for Domiziano and Nerone the left area is the one near the photomultiplier, instead for Tito the left area is the one where there is the exit cable.

Table 2.3: Display of the uniformity results

N_{triple}/N_{double}	N_{triple}/N_{double}	...
Efficiency ± Error	Efficiency ± Error	...

2.2.3.1 Tito

The data are reported in Table 2.4 and the uniformity is verified within the uncertainties.

Table 2.4: *Scanning along Tito*

100/142	135/193	155/223	148/216	126/193
70 ± 4 %	70 ± 3 %	70 ± 3 %	69 ± 3 %	65 ± 3 %

2.2.3.2 Domiziano

The data are reported in Table 2.5 and the uniformity is verified within the uncertainties.

Table 2.5: *Scanning along Domiziano*

77/79	76/80	77/79	82/89	57/60	54/60	70/78
97 ± 2 %	95 ± 2 %	97 ± 2 %	92 ± 3 %	95 ± 3 %	90 ± 4 %	90 ± 3 %

2.2.3.3 Nerone

The data are reported in Table 2.6. Differently from Domiziano and Tito, Nerone shows more pronounced differences between the areas, even though it is possible to agree upon its general uniformity since there are not differences between the areas of too many σs. However, in retrospect, this could have been seen as a hint to immision of external light which will be treated in Section 2.4.

Table 2.6: *Scanning along Nerone*

65/85	68/103	68/85	73/87	59/82	63/92	56/79
76 ± 5 %	66 ± 5 %	80 ± 4 %	84 ± 4 %	72 ± 5 %	68 ± 5 %	71 ± 5 %

2.3 Calibration of electronic equipment

Before setting up the trigger circuit, a characterization of the electronic chain is necessary. For this purpose the behaviour of the delay, logic and coincidence unit must be studied. It will also be analyzed the response of the discriminator together with some considerations about the pulse shapes, and the digitizer.

2.3.1 Delay unit

In order to test the delay unit linearity the simple circuit in Figure 2.9 is required. After splitting the NIM signal coming from the discriminator with a fan-in/fan-out module, one branch goes directly to one channel of the oscilloscope, while the second one is delayed by a chosen amount of nanoseconds and then connected to another oscilloscope channel. The two signal will appear displaced in time.

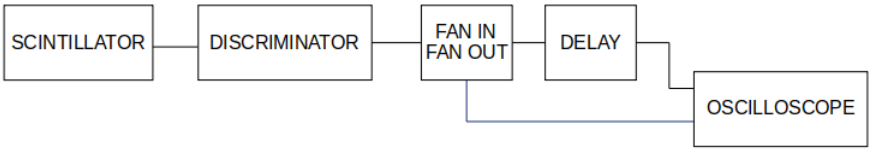

Figure 2.9: *Scheme for delay unit characterization*

The cables are chosen in a way that the initial delay is due to the dead time of the delay unit ($\sim$ 2,5 ns). The calibration is obtained varying the delay on the unit and comparing it with the one read on the oscilloscope. The plot is shown below in Figure 2.10. The non-linearity in this case is negligible.

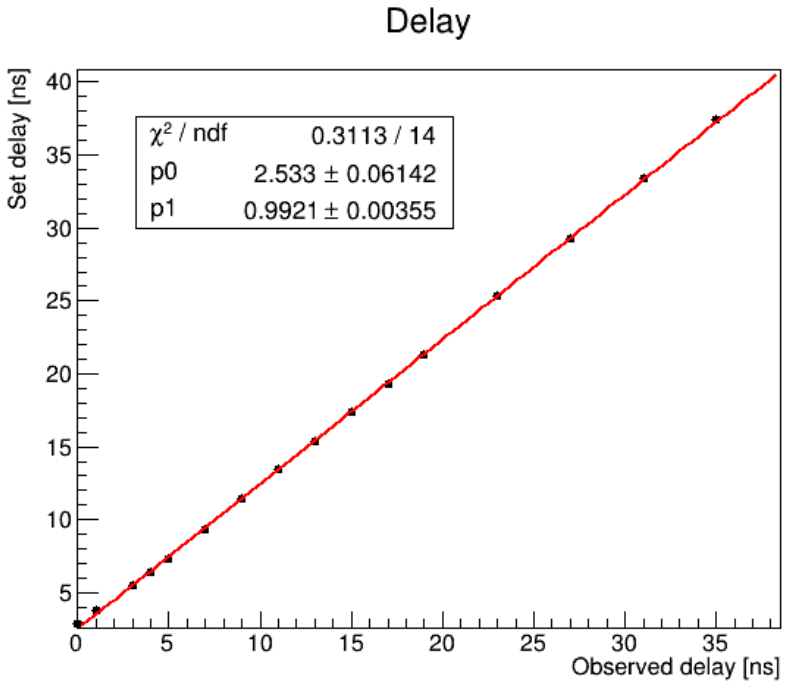

Figure 2.10: *Delay linearity*

2.3.2 Logic unit

The logic unit is the module which permits to make boolean operations (AND, OR, NOT) between signals. In this case, two NIM signals (65 ns wide) enter the logic unit in AND mode. One signal is displaced in time with a delay unit, while the other goes directly from the Fan-In/Fan-Out module to the logic unit. The circuit is shown in Figure 2.11. The logic unit gives back an output if the two signals are overlapped until

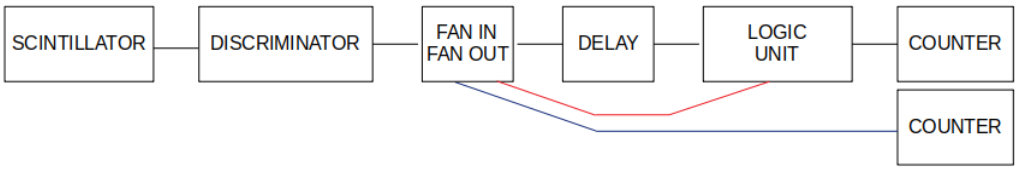

Figure 2.11: *Scheme for logic unit characterization*

few nanoseconds. The purpose is to quantify its response, comparing the counts obtained in the two channels of the counter. The plot is shown in Figure 2.12.

The function used to fit is empirical:

$$f(t) = \frac{f_0}{1 + e^{k(t-t_0)}} \tag{2.7}$$

where f_0 is the asymptotic value of f(t) for small t and t_0 is the time at which f(t) =

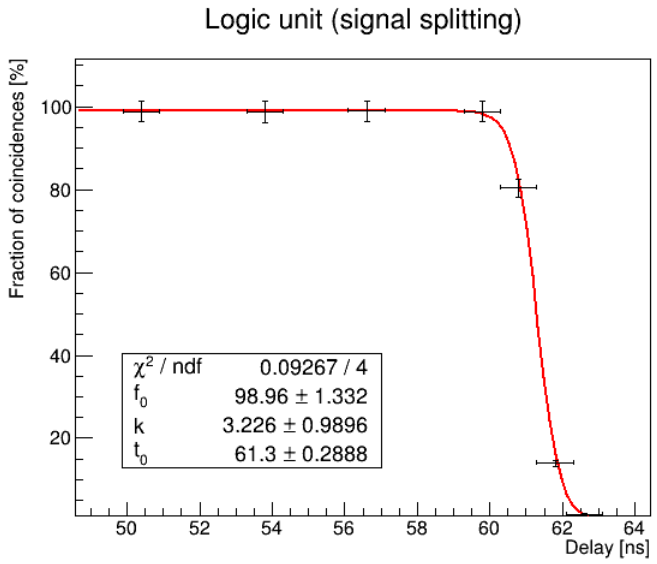

Figure 2.12: *Logic unit characterization with a single splitted signal*

$0.5f_0$; k is a constant value. It can be observed that the counts fall quite sharply around 60 ns and almost no counts (<2%) are registered for delays greater than 62.5 ns. The logic unit starts to give outputs when the two signal are overlapped for at least 5 ns.

Almost the same strategy can be applied to two signals coming from two different scintillators, as shown in Figure 2.13.

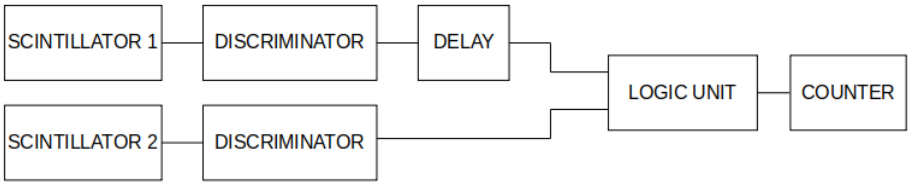

Figure 2.13: *Scheme for logic unit characterization with two scintillators*

When dealing with two scintillators, casual coincidence must be taken into account. The casual coincidence rate (for small τ, here $\tau = 65$ ns) is:

$$R_{casual} = 2\tau R_1 R_2 \tag{2.8}$$

where R_1 and R_2 are the events rate in the two scintillators. Here R_1, $R_2 < 30$ Hz, which gives $R_{casual} < 10^{-4}$ Hz, negligible. The plot is shown in Figure 2.14. It can be noticed that in this case the fall in the number of counts is less abrupt (~ 10 ns), due to stronger effects of time jitter and amplitude walk, which can be expected if two different scintillators are used. The parameter t_0, however, is comparable to the one obtained with a splitted signal.

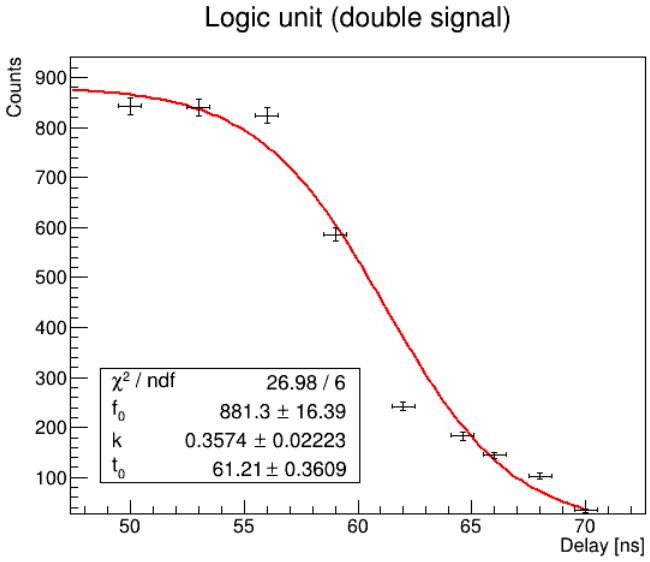

Figure 2.14: *Scheme for delay unit characterization*

2.3.3 Coincidence unit

The same approach used with the characterization of the logic unit can be applied to the coincidence unit. The circuit is equivalent to the one set up for the logic unit and it is shown in Figure 2.15. The NIM signal width is always 65 ns. The number of counts

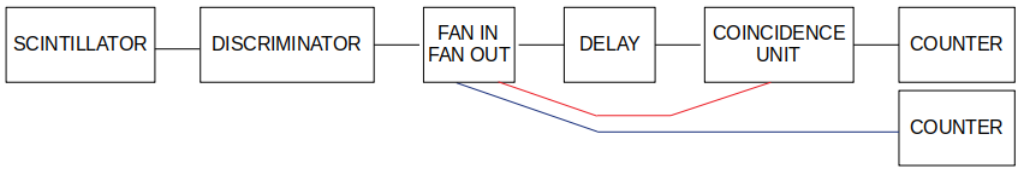

Figure 2.15: *Scheme for coincidence unit characterization*

registered by the first counter are represented as percentage of the total counts registered by the second counter. The fitting function is always Equation 2.7. Here, it takes 2.5 ns to fall from the 90% to the 10% of the total number of counts, as shown in Figure 2.16.

As before, the coincidence unit can be studied with two signals coming from two different scintillators. The result is plotted in Figure 2.17.

Now, as it will be understood in the next section, it is important to study the coincidence unit in anti-coincidence mode. After multiplying the signal via a Fan-In/Fan-Out, one of them is widened up to 130ns and changed in a logic Active-Low signal with a Dual Timer unit. The original signal joins the other one in the coincidence unit after being first anticipated and then delayed, gradually.

As expected, the number of coincidence counts fall abruptly when the signal are

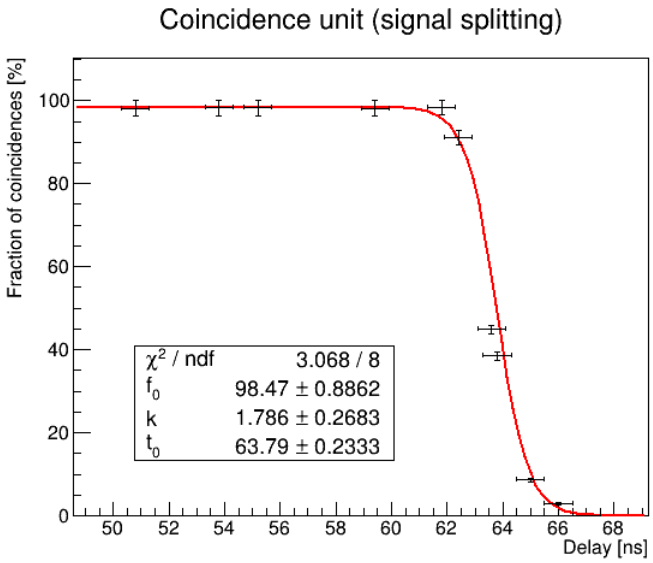

Figure 2.16: *Coincidence unit characterization with two scintillators*

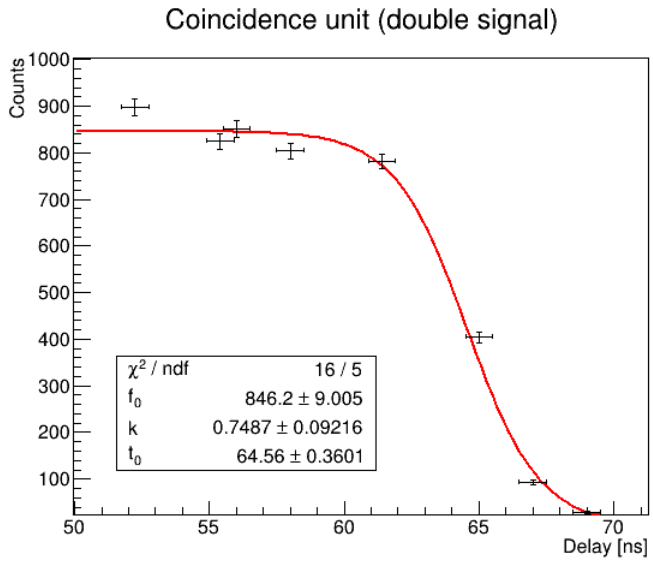

Figure 2.17: *Coincidence unit characterization with two scintillators*

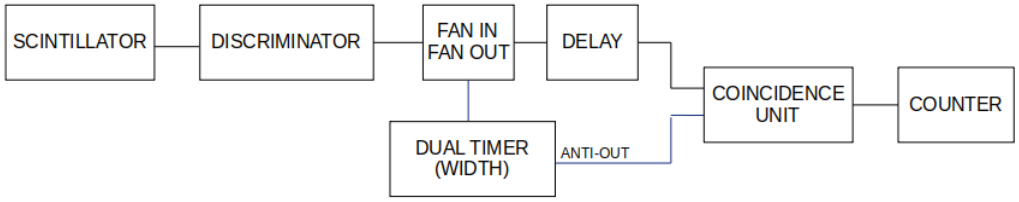

Figure 2.18: *Scheme for coincidence unit characterization (anti-coincidence)*

overlapped completely (this occurs starting from 0 up to 130 ns, see Figure 2.19). When dealing with an anti-coincidence operation, spreading the Active-Low signal is fundamental because the original signal must fall completely in the "valley" of the other one and temporal shifts may occur due to electronic noise.

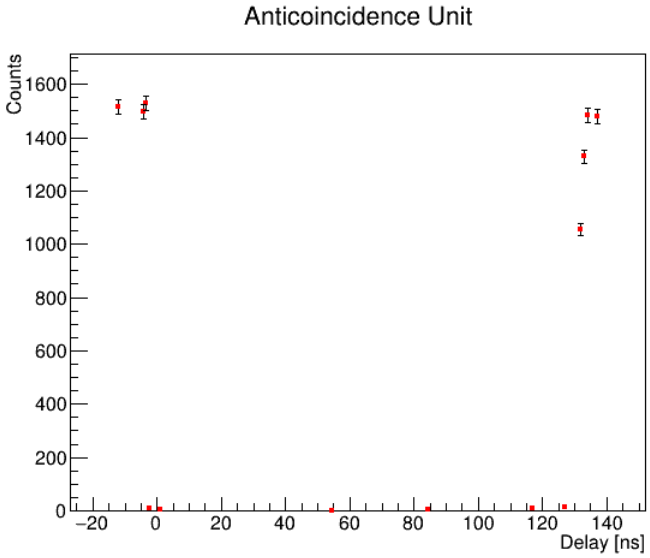

Figure 2.19

2.3.4 Discriminator

In this experiment, signals coming from the scintillators go directly to the discriminator channels. The discriminator is the only module which deals with the analogic shape of the pulse. Once a threshold is selected, this module gives a NIM output only when the signal amplitude is greater than the selected one. However, due to the noisy and spiky shape of the signals the discriminator showed some problems in detecting the pulses, losing some events. We also tried to clean the signal by applying a passive filter to the pulse without significant improvements. Pulse shapes for the three scintillators are shown in Figure 2.20. We will talk more about these problems in Section 2.4.

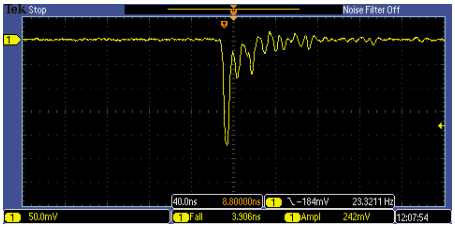

(a)

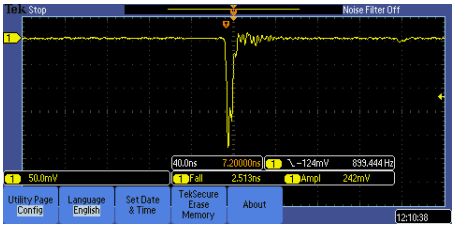

(b)

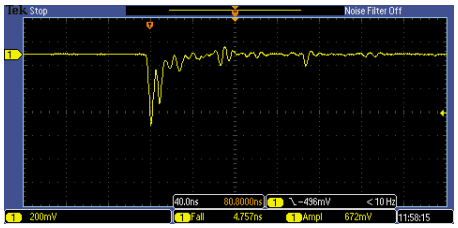

(c)

Figure 2.20: *(a) Nerone, (b) Tito, (c) Domiziano*

2.3.5 Digitizer

The last electronic device that must be characterized is the digitizer, which allows us to make an off-line analysis of the triggered signals coming from the scintillators. The CAEN DT5751 is a 2-4 Channel 10 bit 2/1 GS/s Desktop Waveform Digitizer with 1 Vpp dynamic range on single ended MCX coaxial input connectors.
Its characterization requires a function generator which produces square signals at variable time distance. This time distance is measured by the oscilloscope and by the digitizer (data produced by the digitizer are read through a program reported in Appendix C). The results of the calibration is shown in Figure 2.21.

The intercept of the fitting line is of no importance since it is compatible with zero and it causes a constant shift in the experimental data anyway. Considering that we will fit with exponential functions, a shift will not affect our results. For what concern linearity, our calibration assures a maximum non-linearity of about 0.1%, by far over the precision of our results. This is the reason why the non-linearity will not be taken into account during the later analysis.

2.4 External light in Nerone

During the experiment we started to notice substantial discrepancies between measurements taken in different days. We thought that might be due to a discriminator instability, so we decided to test each of its channels. The first test we performed was to count square waves produced by a pulser and comparing the number of counts with the expected frequency. We did not notice discrepancies, proving the correct functioning of the module with clear and wide signals. The next step was to verify the aforementioned

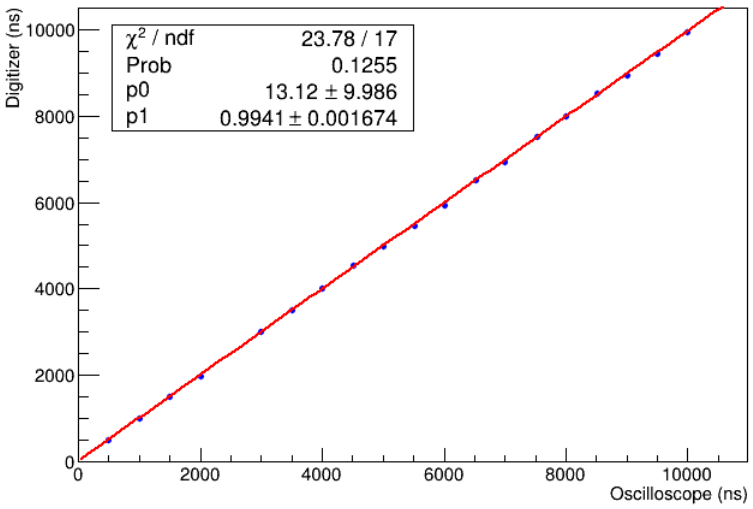

Figure 2.21: *Digitizer linearity*

stability with real analogic signal. Another discriminator was provided in order to compare the measurements; this will be indicated as "good discriminator" from now on, while "old discriminator" is the one of the experiment. The test consists of counting the events detected from a scintillator in 45 seconds, both with the good and the old discriminator, and repeating it on different days. This test has been made for each of the scintillators used in the experiment. We also measured the "experimental threshold", the point upon which events are actually detected. This value is generally far higher than the one that has been set in the discriminator and can be determined with the oscilloscope. All the data are reported in Appendix A, here we just draw the conclusions.

Both discriminators operate quite well as long as they receive a clean signal, like Caracalla's. On the contrary, some channels seem to have problems while counting the events coming from Nerone and Domiziano, whose signals have a quite uneven shape. Since we had used different channels on different days, this probably explains the discrepancies we observed in the first part of the experiment. As a consequence, these measurements allowed us to identify the best functioning channels of the discriminator for each detector.

We also noticed the signal causing most inaccurate countings was Nerone's; that was probably due to a quite noisy baseline in addition to the problem related to the shape of the signal. After a few investigations, we were able to understand the issue was due to light penetrating in one end of the detector, which we subsequently covered. This made the baseline clean, reducing the problems to the shape of the signal.

Chapter 3

Lifetime measurement

3.1 Trigger system

To acquire only muon events it is necessary to build a trigger chain as the one in figure 3.1. The trigger system provides an External Trigger signal for the Digitizer. The signal consisted in the logic coincidence (AND operation) between a START and a STOP, marking respectively the decay of a particle in the middle scintillator and the release of energy, by the charged decay product, in one of the external detectors.

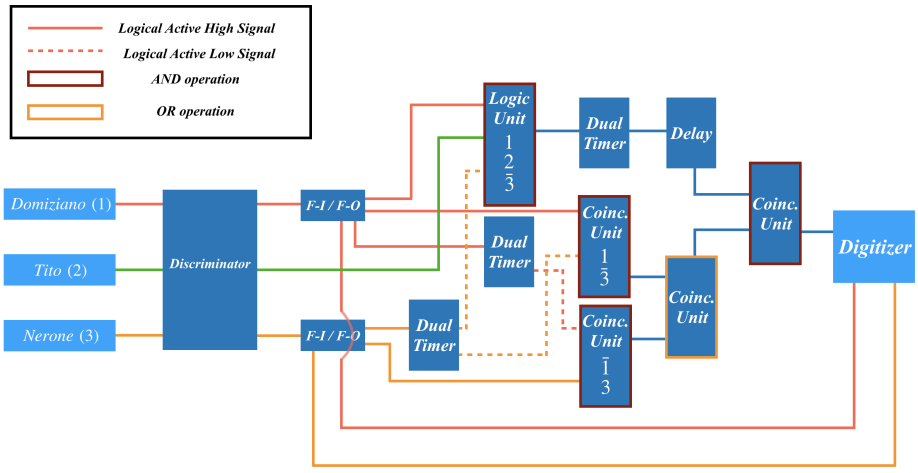

Figure 3.1: *Scheme of the trigger production logic chain.*

3.1.1 Start

The START signal corresponds to the capture of the muon in the middle scintillator, this involves the release of energy in the upper two detectors and not in the lower one. To

produce the START, pulses from the scintillators are inserted in the Discriminator Unit and its outputs are multiplied with a Fan-In/Fan-Out Unit. The lower detector signal is widened and changed in a logical Active-Low one with a Dual Timer Unit. Then the three pulses are sent to a Programmable Logic Unit to perform logic AND operation. The widening of the logical Active-Low signal is necessary to prevent fake coincidence event caused by time shifts due to the electronic noise. Its output is extended *via* the Dual Timer till the period of time in which we expect the selected muons to decay (10 μs).

3.1.2 Stop

The STOP signal corresponds to the loss of energy of the charged lepton produced in the decay in one of the outer scintillators. The signal may though come from both upper and lower detector and the two possibilities must be taken into account.
To produce the STOP signal a Quad Coincidence Unit is used. Its upper two channels are set to perform an AND operation between the signals from the external detectors: one "normal" and the other extended and changed in Active-Low in the first channel, and the opposite in the second one (figure 3.1). The outputs of these operations are then put in the third channel, set to perform an OR operation between the two STOPs.

Finally, it is performed a logical AND between the overall STOP and the widened START signals. The START signal is delayed of $\sim 50ns$ to prevent fake Trigger events caused by auto-coincides (since a START signal is also a STOP's).

3.1.3 Comments

To perform anti-coincidence operation the main signal must fall completely in the middle of the Active-Low one, so the latter is widened. This operation, made with a Dual Timer Unit, delays the signal of a brief amount of time ($\sim 20\ ns$) and arises the need to delay the main signal as well. Due to the lack of performing Delay Units this delay is added using LEMO cables though this procedure deformed slightly the shape of the signal.

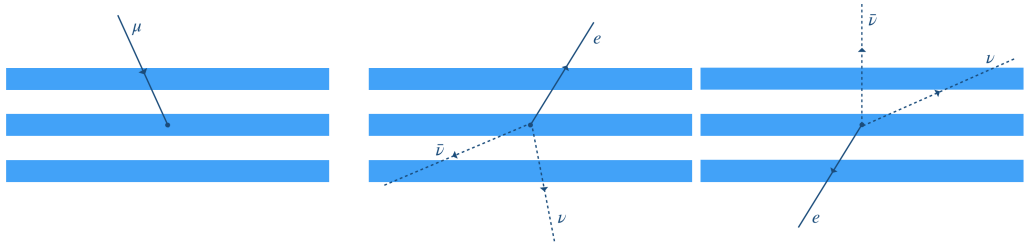

(a) (b)

Figure 3.2: *Scheme of one possible decay event, (a) The incident muon stops in the middle scintillator. (b) The muon decays activating the upper or lower scintillator.*

3.2 Data analysis

Offline data anlaysis has been made on the triggered signals of the scinitillators. The digitizer produces a XML file which contains the digitized waveform. A C++ code reads the XML file and calculates the Δt between the signals (see Appendix C). Additionally, the code allows us to distinguish between a stop in the upper or lower scintillator. An histogram is filled with the various Δt and we expect an exponetial trend:

$$N(t) = N_0 \; e^{-\frac{t}{\tau}} + C \tag{3.1}$$

where τ is the muon lifetime and C is the uniform background due to random coincidences.

3.2.1 Background

It is possible to make prediction about the expected uniform background since it is caused by random signals satisfying the trigger requirements. We need to know the width of the coincidence gate ΔT = 10μs, the rate in the outer scintillators (r_1, r_2) and the rate of starts. The probability of having an uncorrelated stop is given by:

$$P = (1 - e^{-r_1 \Delta T}) + (1 - e^{-r_2 \Delta T}) \tag{3.2}$$

Since in our situation $r_i \Delta T \ll 1$, the following approximation is useful:

$$P \simeq (r_1 + r_2)\Delta T \tag{3.3}$$

In each bin of width $dt \ll \Delta$T:

$$P \simeq (r_1 + r_2) dT = constant \tag{3.4}$$

The expected continuous background can be calculated straightforwardly knowing how last the run (T):

$$C = r_{bkg} \cdot T = P \cdot r_{start} \cdot T \tag{3.5}$$

3.2.2 Estimation of the measured lifetime

Since our apparatus cannot distinguish between μ^+ and μ^-, we will measure a lifetime which should lie in the middle of τ_{μ^+}=2197ns and τ_{μ^-}=2026ns. We have developed a MC simulation which gives an estimate of the lifetime we expect to measure. In the next lines the idea behind such MC is explained.
The MC generates a "number of events" from a Poisson distribution with mean value equal to the number of events in the data set. This "number of events" is divided in N^+ (number of μ^+ events) and N^- (number of μ^- events) using a Binomial distribution. The percentages of μ^+ and μ^- are, respectively, 56% and 44%. The next step is to generate N^+ events with a lifetime equal to τ_{μ^+} and *mutatis mutandis* with N^-. An histogram is filled with all the events and fitted with the function (3.1) - the background is not

simulated. This algorithm is repeated many times, and each time a different lifetime with its uncertainties is obtained. The value to compare with the experimental result is τ_{MC} and it is obtained with the weighted mean.
The charge ratio is not an exact number, its measurent gives the value 1.25±0.03 [5]. This means that the percentages of μ^- and μ^+ should be varied within the uncertainties of the charge ratio, and the change in τ_{MC} should be taken into account as a systematic. The estimated difference in lifetime due to this effect is too small, by far over the precision of our measurements, so it is neglected in our analysis.

3.3 Run 1

Nerone (TOP)	th: 150 mV/HV: 1000V
Tito (MIDDLE)	th: 50 mV/HV: 1200V
Domiziano (BOTTOM)	th: 110 mV/HV: 1000V
Time	15 days
τ_{MC}	2102.87± 0.10(stat) ns
C_{exp}	5.18

Table 3.1: *Run 1 set up*

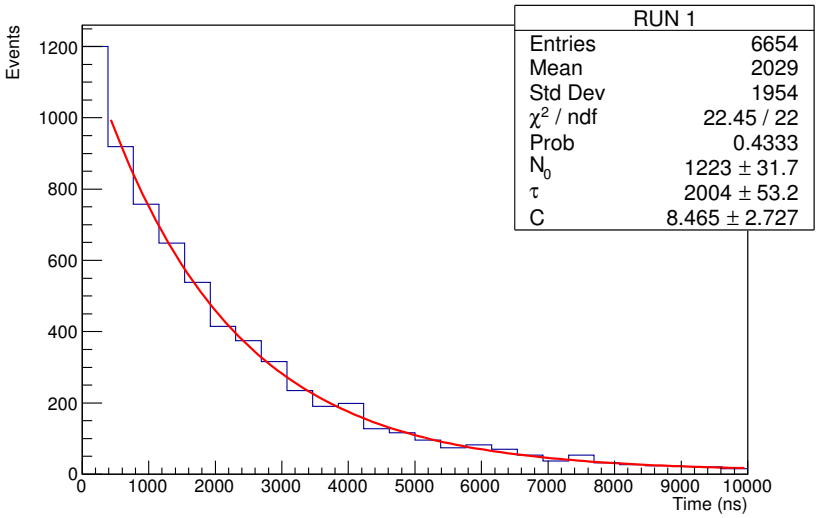

Figure 3.3: *τ distribution during Run1. The first bin is not included in the range of fit since it is affected by the delay to reduce the autocoincidence.*

The experimental result is:

$$\tau_{run1} = 2000 \pm 50\ ns$$

The result is not between $\tau_{\mu+}$ and $\tau_{\mu-}$ as expected, but it is in agreement with τ_{MC} within $\sim 2\sigma$. The measurement of the background ($C = 8 \pm 3$) is in complete agreement with the theoretical calculation.

3.3.1 Stability

The number of bins and the range of fit should be chosen to make the fit results almost independent from their choices, to make the reduced-$\chi^2 \sim 1$ and to guarantee enough statistics in each bin. Figure 3.4 shows the reduced-χ^2 as a function of the number of bins and the final point of the range of fit (we only change the final point and not the initial one since we have an exponential behaviour, cutting the first bins means removing a lot of events). The plot does not show an overall stability but we can notice some subareas in which there is. Since we want a reduced-$\chi^2 \sim 1$ we have decided to perform the fit in the region at low bins.

Figure 3.5 shows the values of χ^2/NDF and τ_μ as functions of the number of bins; this time, a narrow range has been considered (from 10 to 60 bins). The histogram used for data analysis has 25 bins, which turned out to be one of the best choices for the χ^2 value. Taking the errors into account, the number of bin does not affect the value of τ_μ. A similar analysis has been made in Figure 3.6, observing the changing of χ^2/NDF and τ_μ with different lengths of the fit range with fixed number of bins (25). The range used for our data analysis has both a reasonable χ^2 value and a smaller uncertainty on lifetime estimation, if compared to the other ranges.

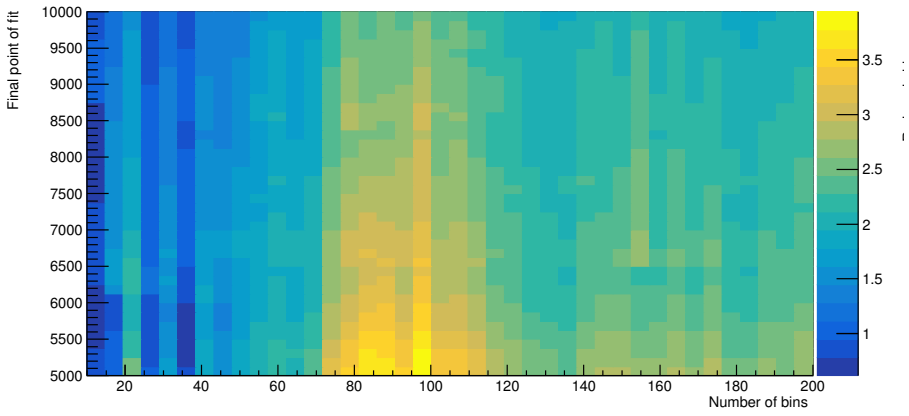

Figure 3.4: *Reduced χ^2 as a function of the number of bins and the final point of fit for Run1.*

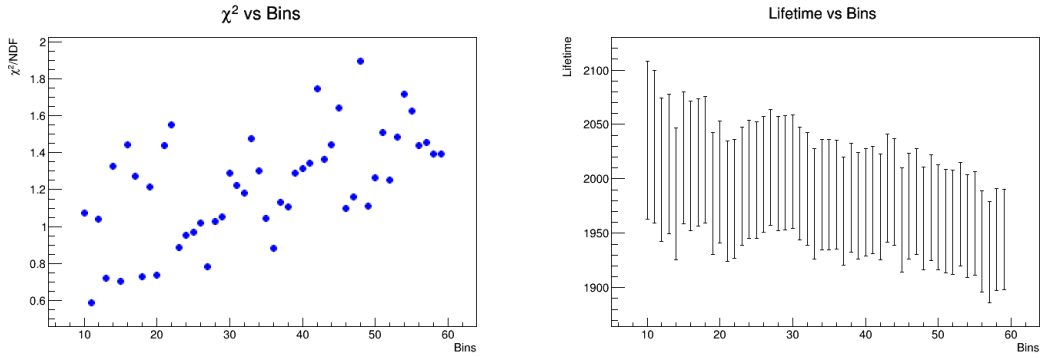

(a) (b)

Figure 3.5: *Values of χ^2/NDF (a) and τ_μ (b) as functions of the number of bins.*

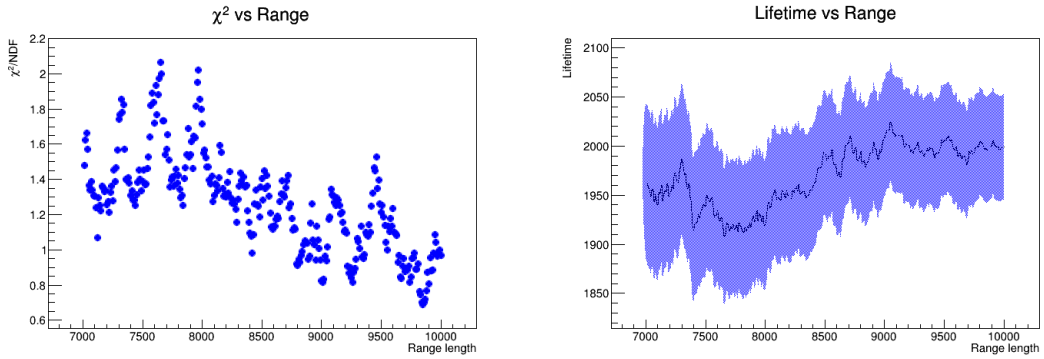

(a) (b)

Figure 3.6: *Values of χ^2/NDF (a) and τ_μ (b) as functions of the fit range length.*

3.3.2 Up and down stop

Since our result is slightly underestimated, we have divided the dataset in events with the stop in the upward scintillator and events with the stop in the downward one to find possible systematics due to the scintillators themselves.

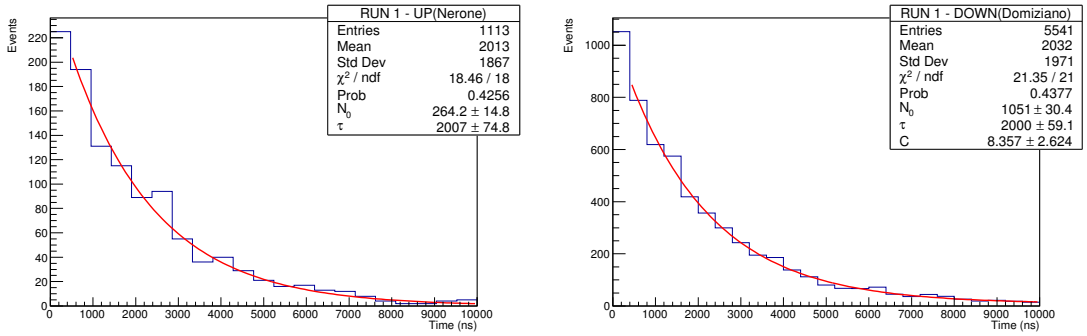

(a) *Upward stops* (b) *Downwars stops*

Figure 3.7: τ^{up} *and* τ^{down} *distribution during Run1. The first bin is not included in the range of fit since it is affected by the delay to reduce auto-coincidences. The continuous background is removed from the fit function of (a). Fitting with the function (3.1) gives* C = *-0.5242± 1.3132 which is highly compatible with zero. Moreover, an analogous theoretical calculation as the one reported in section 3.2.1 (the contribution from the downward scintillators must be removed) gives an expectation of 0.3. Removing a free parameter reduces the uncertainties on the others.*

The results from the separated fit are:

$$\tau^{up}_{run1} = 2010 \pm 70\ ns \qquad \tau^{down}_{run1} = 2000 \pm 60\ ns$$

There is not a relevant difference between τ^{up}_{run1} and τ^{down}_{run1}, they are in agreement with each other and with τ_{run1}, basically they are equal.
An important thing to notice is the large difference in the number of events, the events with a stop from Nerone are only 20% of the total. Figure 3.8 shows the τ distributions near the beginning of the x-axis. It is important to notice the presence of a peak of events around 150ns when the stop signal comes from Domiziano. These features will be treated deeply in the next sections.

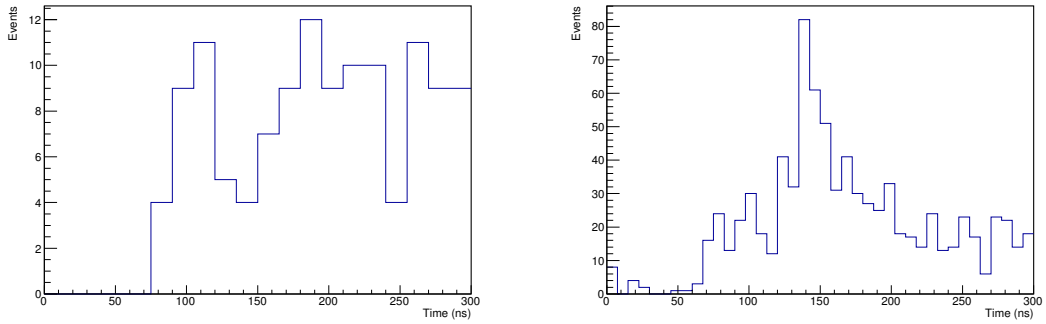

(a) *Upward stops (Nerone)* (b) *Downwars stops (Domiziano)*

Figure 3.8: τ^{up} *and* τ^{down} *distribution during Run1 in the range [0,300]ns.*

3.3.3 μ^- and μ^+ lifetimes

Since negative and positive muons have different lifetimes in matter due to the muon capture (1.4), we tried to estimate τ_{μ^+} and τ_{μ^-} by fitting the data with the sum of two exponential functions:

$$f(t) = N_{\mu^+} e^{-t/\tau_{\mu^+}} + N_{\mu^-} e^{-t/\tau_{\mu^-}} + C \tag{3.6}$$

where C is a constant representing the background. This analysis has been made by fixing one of the two lifetimes and leaving the other one free, in order to reduce the uncertainity on the parameters. The results are in good agreement with the tabulated values (see Figure 3.9 and Table 3.2).

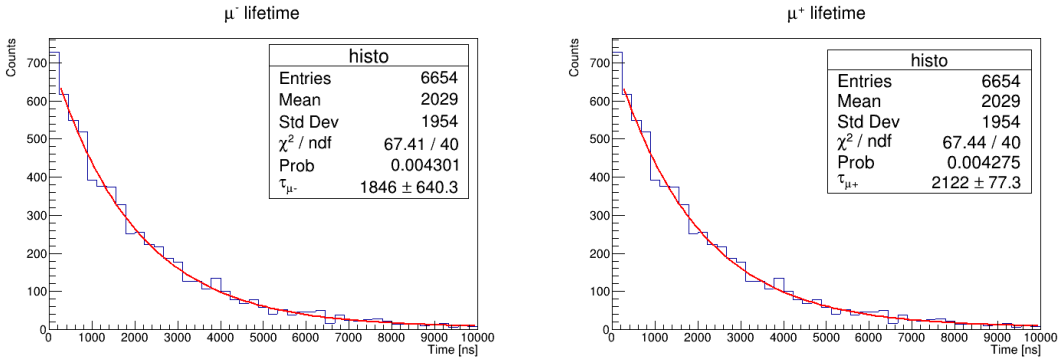

(a) μ^- *lifetime* (b) μ^+ *lifetime*

Figure 3.9: μ^- *and* μ^+ *lifetime estimation.*

Table 3.2: *The first column of the table shows the tabulated values for negative and positive muons' lifetimes in carbon. The fit results are listed in the second column.*

τ_{μ^-} (tabulated value)	τ_{μ^-} (fit)
2.026 μs	1.8 μs $\pm$ 0.6
τ_{μ^+} (tabulated value)	τ_{μ^+} (fit)
2.197 μs	2.12 μs $\pm$ 0.08

3.3.4 Time resolution

We have also investigated another potential source of systematic due to time resolution. When the electron/positron flies downward, the C++ code, reported in Appendix C, measures the time difference between the START signal, which is from the top scintillator, and the STOP signal, which is from the bottom scintillator. Different behaviours and different working points of Nerone and Domiziano could lead to the increase or reduction of the measurement of the time interval between them.
To quantify such phenomenon we have taken coincidence events from the top and bottom scintillator, and we have measured their distance with our code. Theoretically, it should be zero; experimentllay, it should be a Gaussian distribution. The results are plotted in Figure 3.10.

As it could be inferred from the reduced-χ^2 (35,7), the fit is of poor quality. The sensibility of the digitizer is 1ns, too big to carry out efficiently such measurement (it is useless to increase the number of bin over 20). We have decided to not consider such systematic because it would have been based upon weak statistical basis, and it is negligible anyway (it is a small fraction of muon lifetime).

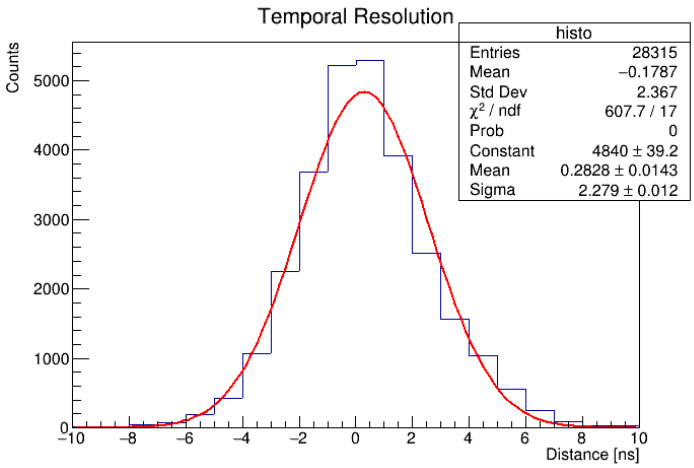

Figure 3.10: *Time resolution.*

3.4 Run 2

Since our experimental setup is asymmetric due to different shapes and behaviours of the scintillators, and since Run1 shows a strong asymmetry in number of "upward stop" and "downward stop" events, during the second Run the position of the outer scintillators are exchanged.

Nerone (BOTTOM)	th: 150 mV/HV: 1000V
Tito (MIDDLE)	th: 50 mV/HV: 1200V
Domiziano (TOP)	th: 110 mV/HV: 1000V
Time	$\sim$ 1 week
τ_{MC}	2114.68$\pm$0.05ns
C_{exp}	$\sim$ 25

Table 3.3: *Run 2 set up. During the Run a blackout occurred, so the exact period of the Run cannot be stated and the expected background cannot be calculated. The latter calculation is performed assuming 6 days as the duration of the run. It is used in the analysis just to fix and compare the order of magnitude.*

A priori we do not expect big changes. Even though the rate of Domiziano is larger than Nerone's, that means more start signals, the trigger chain should guarantee the selection of muon events. Naturally, we also expect a bigger background due to coincidences triggered by noise and/or other radiations, but this should be continuous and easy to calculate (see Section 3.2.1).
However, the situation is different from what expected. First of all, the experimental result is completely incompatible with our expectations:

$$\tau_{run2} = 1059 \pm 27\ ns$$

Secondly, the χ^2 is a little worse than the previous run, inferring the presence of something which "dirty" the exponential trend (to obtain an acceptable value we need to cut the range of fit to almost 1000ns). Thirdly, the number of events increased considerably: the rate of events during Run1 is $\sim 10^{-3}$ Hz, otherwise during Run2 it is $\sim 10^{-2}$ Hz.
Combining these information we can infer about the presence of spurious signals which cause the growth in events and the underestimation of the lifetime. These signals cannot be from random coincidences, otherwise they would be included in C. Watching carefully at the oscilloscope we saw the presence of afterpulses in the waveform of Domiziano. These afterpulses are usually low-amplitude signals, but sometimes they become comparable with the real one. The time delay between the signal and the afterpulse is usually $\lesssim$ 150ns. Our problems can be explained by such afterpulses since they can be identified as stop signals. This hypothesis is supported by the splitting in "upward stops" events and "downward stops" events, as reported in Figure 3.12(a) and 3.12(b).

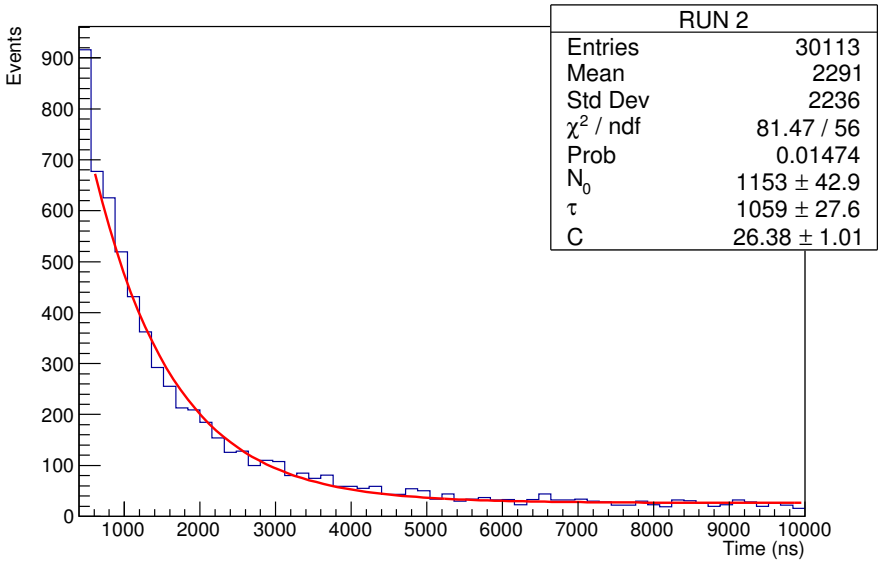

Figure 3.11: *τ distribution during Run2. The x-axis range has a cut between [0;400] ns due to the presence of the peak at 150 ns. The overall plot is in Appendix (....). The first bin is not included in the range of fit to increase the goodness of fit.*

The number of events from a Domiziano stop are the vast majority and the experimental lifetime $\tau^{up}_{run2} = 967 \pm 26$ ns shows the same problems as τ_{run2}.
On the other hand, Nerone shows better results. The uncertainty of the measured lifetime $\tau^{down}_{run2} = 1940 \pm 150$ ns is bigger ($\sim 8\%$) due to the low statistics, but the result is in agreement with τ_{MC}, furthermore it is indicatively a better estimation than τ_{run2} and τ^{up}_{run2}., so Nerone is not the source of the systematics.
The lower pads of Figure 3.12 show another proof in support of our hypothesis. Nerone does not exhibit the peak at 150ns (there is a peak at the beginning of the scale due to the residual autocoincidence, by the way), whereas Domiziano does.

The values of χ^2/NDF and lifetime as functions of the number of bins and range length have been investigated (Figures 3.13 and 3.14), in the same way as has been done for Run 1: we can say τ_μ is not affected by the number of bins if that's bigger than 13, while the χ^2 improves as the number of bins increase. On the contrary, the range length affects the lifetime: considering the whole dataset makes τ_μ get closer to its real value, even if the results are not in agreement with what expected. Differently from Run1, we can see in Fig. 3.14 a slightly instability of the lifetime and a slightly spread of the χ^2, inferring the poor quality of the data.

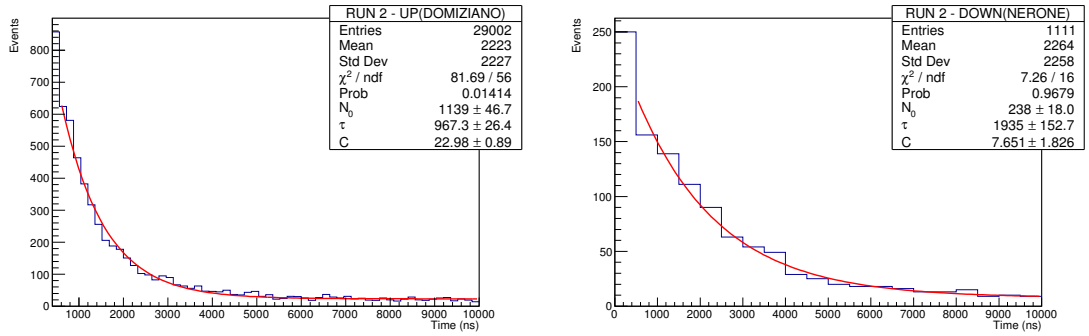

(a) *Upward stops (Domiziano)* (b) *Downwars stops (Nerone)*

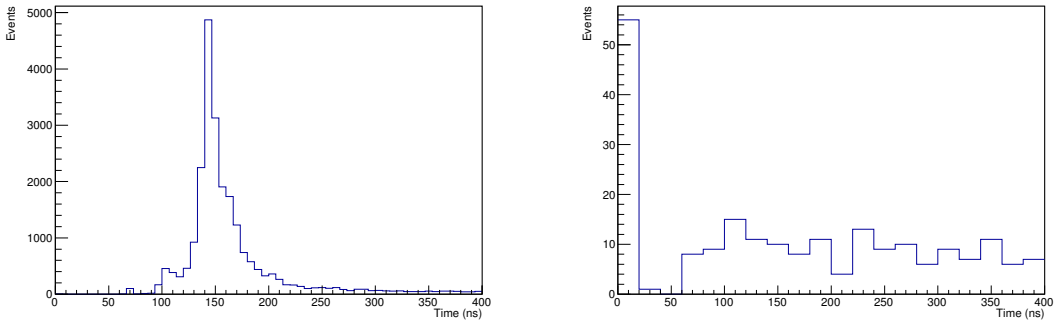

(c) *Upward stops zoom (Domiziano)* (d) *Downwars stops zoom (Nerone)*

Figure 3.12: *In (a) and (b) τ^{up} and τ^{down} distribution during Run2. The first bin is not included in the range of fit to increase the goodness of fit. in (c) and (d) τ^{up} and τ^{down} distribution during Run2 in the range [0,400]ns.*

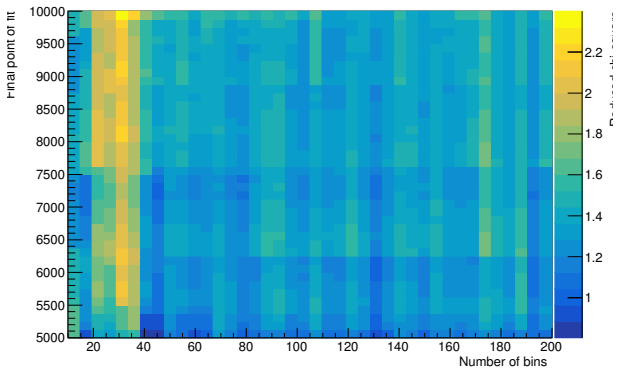

Figure 3.13: *Reduced χ^2 as a function of the number of bins and the final point of fit for Run2.*

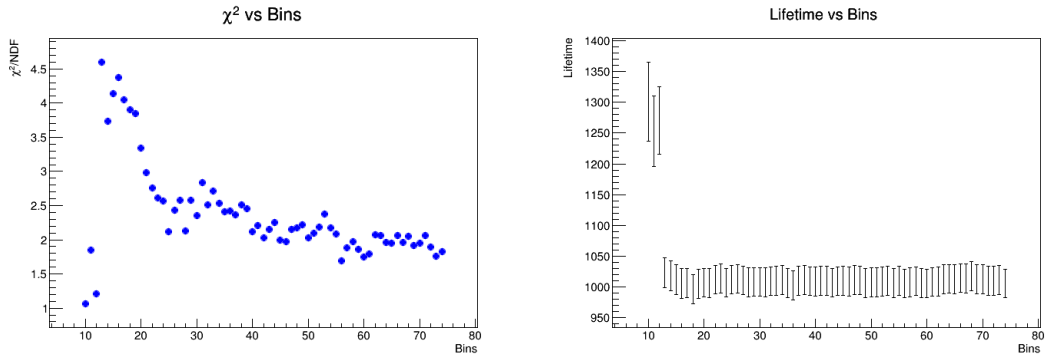

(a)

(b)

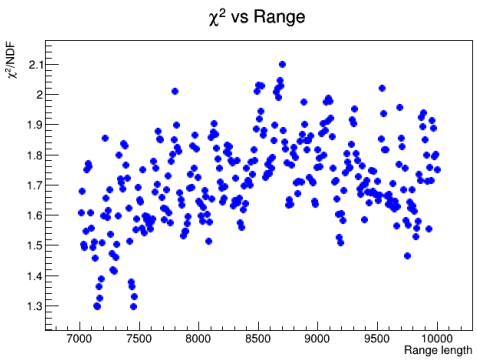

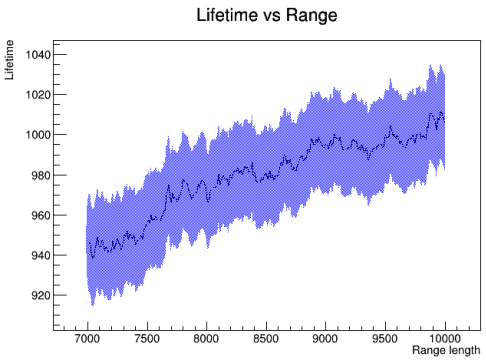

(c)

Figure 3.14: *Values of χ^2/NDF and τ_μ as functions of the number of bins (a). (b) and range length (c), (d).*

3.5 Run 3

In this Run the spurious signals are analyzed deeply and a possible solution to reduce them is investigated. Domiziano's threshold is raised up to 180mV trying to reduce the impact of the afterpulses. This causes an efficiency loss, of course, but it could lead to a better result.

Nerone (BOTTOM)	th: 150 mV/HV: 900V
Tito (MIDDLE)	th: 50 mV/HV: 1200V
Domiziano (TOP)	th: 180 mV/HV: 1000V
Time	————
τ_{MC}	2079.30±0.17ns
C_{exp}	————

Table 3.4: *Run 3 set up. During the Run many blackouts occured, so we cannot report an useful period of time for the calculation of the bakcground.*

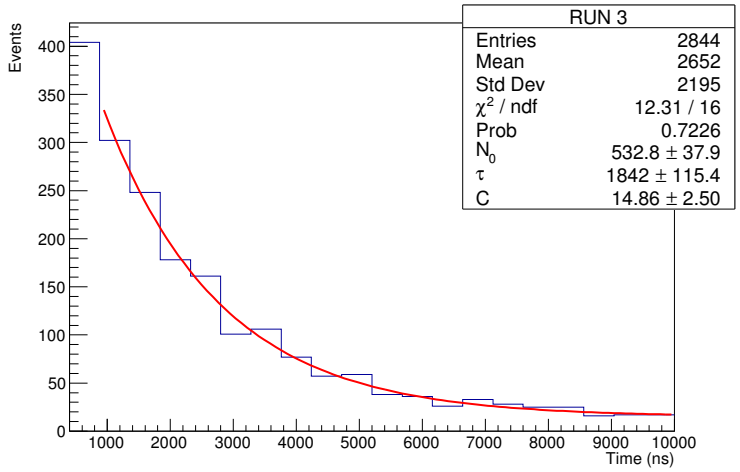

Figure 3.15: *τ distribution during Run3. The x-axis range has a cut between [0;400] ns due to the presence of the peak at 150 ns. The first bin is not included in the range of fit to increase the goodness of fit.*

The experimental result is greatly improved:

$$\tau_{run3} = 1840 \pm 120 \ ns$$

The result is still underestimated but we can notice an improvement towards our ideal experimental expectation. Formally, it is in agreement with τ_{MC} within $\sim 2\sigma$, but the

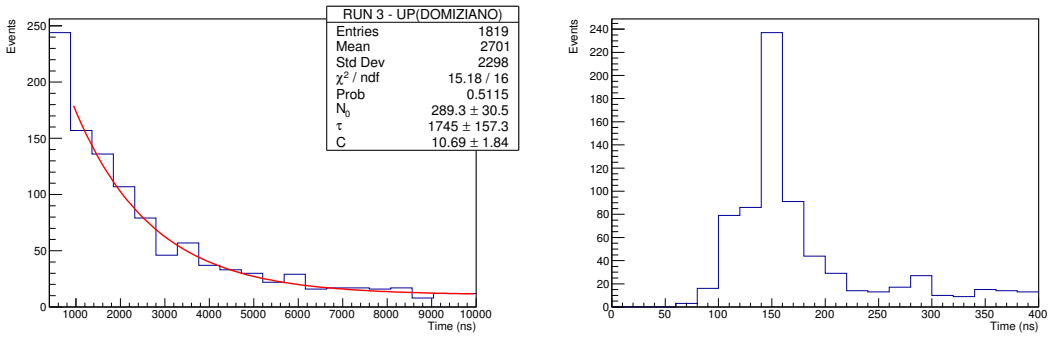

(a) *Upward stops (Domiziano)* (b) *Upward stops zoom (Domiziano)*

Figure 3.16: *In (a) τ^{up} distribution during Run3. The first bin is not included in the range of fit to increase the goodness of fit. in (b) τ^{up} distribution during Run3 in the range [0,400]ns.*

uncertainties is not so small ($\sim$6.5%).
The cons of increasing the threshold is the reduction in efficiency and, over a certain threshold, the number of muon signals which pass the discriminator. To prevent such problems, it could be useful to find a method to reduce the afterpulses getting at the root cause. Afterpulses in a photomultiplier can be generated by many different factors, the easiest and "blind" possible solution is to reduce the HV.
We reduced the HV to 900V and we tried to take data with this new configuration. The rate of events suffered a great reduction and, with the available time and the blackout problems, we were not able to take enough data to do a rigorous analysis. However, we can report a general observation: from the analysis of the waveform with the oscilloscope we saw a reduction, almost a disappearance, of the afterpulses.

Chapter 4

Conclusion

During the experiment we had many problems with the scintillators, so we spent most of the time to investigate and find the sources of such problems and possible solutions rather than taking data.

To sum up, our problems were not mainly caused by the electronic chain that seemed to work properly. There is only two exceptions for what concern the delay unit and discriminator. We used two different delay units and they both have the problem of distorting significantly the shape of the waveform, causing many problems and the need to use many LEMO cables to delay signals. Another problem was due to the discriminator that triggered signals over the set threshold; this was caused by the narrow width and uneven shape of the signals. However, once the problem was identified, it did not create big concern. Additionally, many channels of the discriminator were not well-functioning.

When we began to take data the set up of the experiment changed a little from the characterization made at the beginning. From the characterization to the first Run, we fixed some problems that could have been caused changes in the optimal working point.

We can identify the scintillators as the main source of our problems, especially noisy baselines and potential reflections. Especially, Domiziano's afterpulses affected our measurements, as discussed in Run2/Run3.
Differently from the other group working on muons, our scintillators were thinner (1 cm vs 4 cm). Muons lost less energy, so they were more difficult to distinguish from the background, and the rate of events were less than "normal" (if the muons lose less energy, their stop in the middle scintillator is less probable).
The other big problem regarding detectors is their bad waveform, we tried to clean it using passive filters but it was useless. Many problems were due to the external light in Nerone and the too high Domiziano's HV. After fixing them, the experimental situation improved.

Despite all the problems, the results are good, especially Run1. The underestimation

of the lifetime in Run1 can be ascribe to Domiziano's afterpulses and low statistics. If we had time to take enough data after Run3, we are confident that we would have had a good result as Run1's, or even better since we had reduced the HV to reduce afterpulses.

Appendices

Appendix A

Discriminator Stability

A.1 Caracalla

Experimental measurements concerning the events detected by Caracalla are listed in Table A.1, A.2, A.3, A.4, A.5 and A.6.

Table A.1: March 28th, 2019; good discriminator.

Channel	Threshold	Counts (mean)	Experimental threshold
CH2	150	41 ± 4	210
CH2	50	340 ± 11	80
CH4	150	38 ± 4	210
CH4	50	342 ± 11	80
CH5	150	33 ± 3	210
CH5	50	356 ± 11	80
CH6	150	35 ± 3	210
CH6	50	341 ± 11	76
CH7	150	32 ± 3	212
CH7	50	326 ± 10	82
CH8	150	32 ± 3	214
CH8	50	296 ± 10	80

A.2 Domiziano

Experimental measurements concerning the events detected by Domiziano are listed in Table A.7, A.8, A.9 and A.10.

Table A.2: March 28th, 2019; old discriminator.

Channel	Threshold	Counts (mean)	Experimental threshold
CH1	150	32 ± 3	226
CH1	50	268 ± 9	88
CH3	150	29 ± 3	230
CH3	50	246 ± 9	92
CH4	150	27 ± 3	236
CH4	50	250 ± 9	88
CH5	150	52 ± 4	200
CH5	50	378 ± 11	76
CH6	150	34 ± 3	204
CH6	50	345 ± 11	80

Table A.3: April 3rd, 2019; good discriminator.

Channel	Threshold	Counts (mean)	Experimental threshold
CH2	150	40 ± 4	200
CH2	50	351 ± 11	76
CH4	150	40 ± 4	196
CH4	50	342 ± 11	74
CH5	150	35 ± 3	205
CH5	50	357 ± 11	72
CH6	150	44 ± 4	205
CH6	50	344 ± 11	74
CH7	150	43 ± 4	208
CH7	50	330 ± 10	73
CH8	150	44 ± 4	204
CH8	50	334 ± 11	78

Table A.4: April 3rd, 2019; old discriminator.

Channel	Threshold	Counts (mean)	Experimental threshold
CH1	150	33 ± 3	220
CH1	50	269 ± 9	84
CH3	150	32 ± 3	218
CH3	50	266 ± 9	84
CH4	150	32 ± 3	216
CH4	50	259 ± 9	84
CH5	150	45 ± 4	194
CH5	50	363 ± 11	76
CH6	150	37 ± 4	212
CH6	50	334 ± 11	80

Table A.5: April 5th, 2019; good discriminator.

Channel	Threshold	Counts (mean)	Experimental threshold
CH2	150	40 ± 4	186
CH2	50	351 ± 11	70
CH4	150	39 ± 4	192
CH4	50	329 ± 11	74
CH5	150	46 ± 3	184
CH5	50	353 ± 11	66
CH6	150	42 ± 4	192
CH6	50	356 ± 11	70
CH7	150	38 ± 4	190
CH7	50	345 ± 10	72
CH8	150	37 ± 4	190
CH8	50	350 ± 11	76

Table A.6: April 5th, 2019; old discriminator.

Channel	Threshold	Counts (mean)	Experimental threshold
CH1	150	30 ± 3	204
CH1	50	261 ± 9	80
CH3	150	33 ± 3	202
CH3	50	256 ± 9	82
CH4	150	27 ± 3	206
CH4	50	242 ± 9	78
CH5	150	39 ± 4	182
CH5	50	377 ± 11	66
CH6	150	41 ± 4	192
CH6	50	349 ± 11	70

Table A.7: April 10th, 2019; good discriminator.

Channel	Threshold	Counts (mean)	Experimental threshold
CH2	150	1188 ± 24.3	227
CH2	50	7720.5 ± 62.1	74
CH4	150	1302 ± 25.5	217
CH4	50	7720.5 ± 62.1	89
CH5	150	1247.5 ± 24.9	210
CH5	50	7828 ± 62.5	79
CH6	150	1265.5 ± 25.1	212
CH6	50	7910 ± 62.8	81
CH7	150	1164.5 ± 24.1	237
CH7	50	7143.5 ± 59.7	90
CH8	150	1183 ± 24.3	230
CH8	50	7429.5 ± 60.3	90

Table A.8: April 10th, 2019; old discriminator.

Channel	Threshold	Counts (mean)	Experimental threshold
CH1	150	1095.5 ± 23.4	215
CH1	50	7036.5 ± 59.3	93
CH3	150	1046.5 ± 22.9	245
CH3	50	6343 ± 56.3	86
CH4	150	1039 ± 22.8	232
CH4	50	6274 ± 56	87
CH5	150	1496.5 ± 27.3	189
CH5	50	8873.5 ± 66.6	84
CH6	150	1135.5 ± 23.8	249
CH6	50	7471.5 ± 61.1	83

Table A.9: April 15th, 2019; good discriminator.

Channel	Threshold	Counts (mean)
CH2	150	1207.5 ± 24.5
CH2	50	7673 ± 61.9
CH4	150	1162.5 ± 24.1
CH4	50	7937 ± 62.9
CH5	150	1199 ± 24.5
CH5	50	7989 ± 63.2
CH6	150	1274.5 ± 25.2
CH6	50	8096.5 ± 63.6
CH7	150	1150.5 ± 23.9
CH7	50	7341 ± 60.6
CH8	150	1185.5 ± 24.3
CH8	50	7494 ± 61.2

Table A.10: April 15th, 2019; old discriminator.

Channel	Threshold	Counts (mean)
CH1	150	1060 ± 23
CH1	50	6943.5 ± 58.9
CH3	150	1031 ± 22.7
CH3	50	6478 ± 56.9
CH4	150	1011 ± 22.5
CH4	50	6295 ± 56.1
CH5	150	1520 ± 27.5
CH5	50	9064.5 ± 67.3
CH6	150	1143.5 ± 23.9
CH6	50	7358.5 ± 60.6

A.3 Nerone

Experimental measurements concerning the events detected by Nerone are listed in Table A.11, A.12, A.14, A.15 and A.16.

Table A.11: April 8th, 2019; good discriminator.

Channel	Threshold	Counts (mean)	Experimental threshold
CH2	150	1506 ± 27	268
CH2	50	449373 ± 474	98
CH4	150	1571 ± 28	272
CH4	50	452152 ± 475	96
CH5	150	1665 ± 29	262
CH5	50	541168 ± 520	90
CH6	150	1993 ± 32	258
CH6	50	525259 ± 512	98
CH7	150	1151 ± 24	298
CH7	50	429287 ± 463	98
CH8	150	1363 ± 26	284
CH8	50	384083 ± 438	96

Table A.12: April 8th, 2019; old discriminator.

Channel	Threshold	Counts (mean)	Experimental threshold
CH1	150	1861 ± 31	272
CH1	50	475027 ± 487	96
CH3	150	1232 ± 25	298
CH3	50	312715 ± 395	106
CH4	150	1051 ± 23	278
CH4	50	317405 ± 398	102
CH5	150	14039 ± 84	214
CH5	50	665834 ± 577	78
CH6	150	1571 ± 268	276
CH6	50	386395 ± 440	100

Table A.13: April 9th, 2019; good discriminator.

Channel	Threshold	Counts (mean)	Experimental threshold
CH2	150	2029 ± 32	278
CH2	50	630730 ± 562	90
CH4	150	1296 ± 25	250
CH4	50	561520 ± 530	98
CH5	150	2009 ± 32	278
CH5	50	580531 ± 539	98
CH6	150	2380 ± 34	186
CH6	50	612134 ± 553	98
CH7	150	1368 ± 26	280
CH7	50	453813 ± 476	104
CH8	150	1319 ± 26	254
CH8	50	502351 ± 501	108

Table A.14: April 9th, 2019; old discriminator.

Channel	Threshold	Counts (mean)	Experimental threshold
CH1	150	2299 ± 34	264
CH1	50	453504 ± 476	100
CH3	150	693 ± 19	278
CH3	50	315116 ± 397	116
CH4	150	619 ± 18	255
CH4	50	182244 ± 302	98
CH5	150	980 ± 22	202
CH5	50	234626 ± 343	80
CH6	150	644 ± 18	222
CH6	50	134129 ± 259	88

Table A.15: April 15th, 2019; good discriminator.

Channel	Threshold	Counts (mean)
CH2	150	1625 ± 29
CH2	50	337102 ± 411
CH4	150	1605 ± 28
CH4	50	329076 ± 406
CH5	150	1495 ± 27
CH5	50	418025 ± 457
CH6	150	1976 ± 31
CH6	50	458476 ± 479
CH7	150	1208 ± 25
CH7	50	345256 ± 415
CH8	150	1326 ± 26
CH8	50	370674 ± 431

Table A.16: April 15th, 2019; old discriminator.

Channel	Threshold	Counts (mean)
CH1	150	1532 ± 28
CH3	150	1161 ± 24
CH4	150	1009 ± 22
CH5	150	10801 ± 73
CH6	150	1475 ± 27

Appendix B

Efficiency measures

Table B.1: Nerone efficiency (1000 V). Domiziano (1000 V, 210 mV), Caracalla(1550 V,150 mV). 2 measures of 10 minutes each.

Threshold (mV)	Doubles I	Triples I	Doubles II	Triples II	Efficiency %	Error
130	114	108	90	85	94.6	1.6
140	97	88	103	100	95.6	1.4
150	88	87	103	98	98.0	1.0
160	109	101	69	67	95.3	1.6
170	114	106	91	83	92.3	1.9
180	96	83	91	82	88.5	2.3
190	86	77	82	72	88.7	2.4
200	90	80	100	87	88.0	2.4
210	89	75	96	79	83.5	2.7

Table B.2: Tito efficiency (1100 V). Nerone (1000 V, 210 mV), Caracalla(1550 V,150 mV). 2 measures of 10 minutes each.

Threshold (mV)	Doubles I	Triples I	Doubles II	Triples II	Efficiency %	Error
30	297	264	308	258	86.6	1.4
40	291	221	280	207	75.0	1.8
50	305	194	301	200	65.0	1.9

Table B.3: Tito efficiency (1150 V). Nerone (1000 V, 210 mV), Caracalla(1550 V,150 mV). 2 measures of 10 minutes each.

Threshold (mV)	Doubles I	Triples I	Doubles II	Triples II	Efficiency %	Error
30	281	253	241	225	91.9	1.2
40	279	263	239	194	83.1	1.6
50	255	193	260	195	75.3	1.9

Table B.4: Tito efficiency (1200 V). Nerone (1000 V, 210 mV), Caracalla(1550 V,150 mV). 2 measures of 10 minutes each.

Threshold (mV)	Doubles I	Triples I	Doubles II	Triples II	Efficiency %	Error
30	214	192	201	190	92.7	1.3
40	195	175	186	165	89.2	1.6
50	182	163	198	170	87.9	1.7
60	201	166	198	161	82.0	1.9

Table B.5: Domiziano efficiency (950 V). Nerone (1000 V, 210 mV), Caracalla(1550 V,150 mV). 2 measures of 10 minutes each.

Threshold (mV)	Doubles I	Triples I	Doubles II	Triples II	Efficiency %	Error
80	95	93	103	102	98.7	0.8
90	91	87	93	91	97.1	1.2
100	97	93	110	107	96.8	1.2
110	89	82	90	80	90.7	2.2
120	108	93	104	89	85.8	2.4
130	137	117	115	100	86.1	2.2
140	85	72	93	72	81.4	2.9

Table B.6: Domiziano efficiency (1000 V). Nerone (1000 V, 210 mV), Caracalla(1550 V,150 mV). 2 measures of 10 minutes each.

Threshold (mV)	Doubles I	Triples I	Doubles II	Triples II	Efficiency %	Error
100	117	115	145	144	99.1	0.6
110	171	168	140	138	98.4	0.7
120	151	141	180	167	93.1	1.4
130	127	116	136	126	92.1	1.7
140	131	115	147	129	87.8	2.0
150	146	124	128	107	84.3	2.2

Appendix C

Code

```
/*
 | Il programma legge un file .xml in cui sono salvati dati presi con due
     canali attivi del digitizer.
 | Gli eventi dei due canali vengono salvati in un file .png all'interno della
     cartella "Events", che
 | deve essere creata prima di far andare il programma. Viene inoltre
     calcolata la distanza temporale
 | tra gli istanti di inizio dei due eventi. Le distanze vengono salvate nel
     file "distance.txt".
*/

//c++ -o distance distance.cpp `root-config --cflags --glibs`

#include <iostream>
#include "TH1.h"
#include "TFile.h"
#include "TTree.h"
#include "TApplication.h"
#include "TCanvas.h"
#include "TString.h"
#include <fstream>
#include <algorithm>
#include <vector>
#include <string>
#include <cstdlib>
#include <string.h>
#include <sstream>
#include<TGraph.h>
#include<TF1.h>
#include<TGraphErrors.h>
#include<TMultiGraph.h>
#include<TLegend.h>
#include<TStyle.h>
```

```
#include<TAxis.h>
#include<TLatex.h>

using namespace std;

int main(int argc, char** argv) {

    vector<double> chZero;
    vector<double> chOne;
    vector<double> time;

    ifstream infile;
    infile.open ("MISURA2.xml");

    string line;
    string begin = "<trace";

    int iEv = 0;

    double distance;

    ofstream outFile;
    ofstream outUp;
    ofstream outDown;

    outFile.open("distanceBis.txt", ios_base::app);
    outUp.open("upBis.txt", ios_base::app);
    outDown.open("downBis.txt", ios_base::app);

    while (!infile.eof()) {

        getline(infile, line, ' ');

        //Quando trovi l'evento nel canale zero..
        if(begin.compare(line) == 0) {

            //.. posizionati nel punto in cui cominciano i valori della
                tensione ..
            getline(infile, line, '>');

            double iTime = 0;

            string chZero_event;

            //.. e salva l'evento in una stringa
            getline(infile, chZero_event, '<');

            //Adesso estrai i numeri dalla stringa: salva la stringa in uno
                stream..
```

```
stringstream chZero_ss;
chZero_ss << chZero_event;

string chZero_word;
double chZero_value;

//..fai un loop fino alla fine dello stream..
while (!chZero_ss.eof()) {

    //..estrai una parola..
    chZero_ss >> chZero_word;

    //.. e se   un numero salvala in un vettore
    if (stringstream(chZero_word) >> chZero_value) {

        iTime += 1;

        chZero.push_back(chZero_value);
        time.push_back(iTime);
    }

    chZero_word = "";
}

//Ora trova l'evento nel canale uno..
getline(infile, line, ' ');

while (begin.compare(line) != 0) {

    getline(infile, line, ' ');
}

//.. posizionati nel punto in cui cominciano i valori della
    tensione ..
getline(infile, line, '>');

string chOne_event;

//.. e salva l'evento in una stringa
getline(infile, chOne_event, '<');

//Adesso estrai i numeri dalla stringa: salva la stringa in uno
    stream..
stringstream chOne_ss;
chOne_ss << chOne_event;

string chOne_word;
double chOne_value;
```

```
//..fai un loop fino alla fine dello stream..
while (!chOne_ss.eof()) {

    //..estrai una parola..
    chOne_ss >> chOne_word;

    //.. e se   un numero salvala in un vettore
    if (stringstream(chOne_word) >> chOne_value) {

        chOne.push_back(chOne_value);
    }

    chOne_word = "";
}

//Conta gli eventi
iEv += 1;

//Trova il punto di inizio dei due eventi..
int chZero_dist = 1;
int chOne_dist = 1;

while ( chZero[chZero_dist] != 0 ) {

    chZero_dist += 1;
}

while ( chOne[chOne_dist] != 0 ) {

    chOne_dist += 1;
}


//.. e se start e stop sono su due canali diversi calcola la distanza
if (chOne_dist != 14336) {

    distance = abs(time[chOne_dist] - time[chZero_dist]);
    outDown << distance << endl;

}

double firstSignal = time[chZero_dist];
double checkSignal = chOne_dist;

//Conta il numero di zeri presenti nel segnale (per stimare
    l'errore)

double errZero = 0;
double errOne = 0;
```

```
while ( chZero[chZero_dist] == 0 ) {

    errZero += 1;
    chZero_dist += 1;
}

if ( checkSignal != 14336 ) {

    while ( chOne[chOne_dist] == 0 ) {

        errOne += 1;
        chOne_dist += 1;
    }
}

//cout << "Gli zeri presenti nel primo segnale del canale zero
    sono: " << errZero << endl;
//cout << "Gli zeri presenti nel canale uno sono: " << errOne <<
    endl;

//Se start e stop sono nel canale zero..
if ( checkSignal == 14336 ) {

    while ( chZero[chZero_dist] != 0 ) {

        chZero_dist += 1;
    }

    distance = abs(time[chZero_dist] - firstSignal);
    outUp << distance << endl;

}

outFile << distance << endl;


//Salva in un grafico i valori di questi due eventi
Int_t n = chZero.size();
Double_t x[n], y[n];

for (Int_t i=0; i < n; i++) {

    x[i] = time[i];
    y[i] = chZero[i];
}

TGraph * chZero_graph = new TGraph(n, x, y);
```

```
        for (Int_t k=0; k < n; k++) {

            y[k] = chOne[k];
        }

        TGraph * chOne_graph = new TGraph(n, x, y);

        //I grafici verranno salvati ciascuno in un file .png, nella
            cartella "Events"
     TString graph_name = ("event");
       graph_name += (iEv);
       graph_name += (".png");

        TCanvas *c = new TCanvas(graph_name, graph_name);

        chZero_graph -> SetTitle(graph_name);
        chZero_graph -> GetXaxis() -> SetTitle("Time [ns]");
        chZero_graph -> GetYaxis() -> SetTitle("Channel");
        chZero_graph -> GetYaxis() -> SetRangeUser(-100, 1000);

        chZero_graph -> Draw();

        chOne_graph -> SetLineColor(2);
        chOne_graph -> Draw("SAME");

        //La cartella "Events" deve essere creata prima di far andare il
            programma
        const char * dirname;
       dirname = "/home/federica/Documents/Muoni/Digitizer/Events";
        chdir(dirname);

        c -> Print(graph_name, "png");

        //Torna ora nella cartella dove si trova il file .xml
       const char * directory;
       directory = "/home/federica/Documents/Muoni/Digitizer/";
       chdir(directory);


        //Cancella i dati presenti nei vettori, per salvare un nuovo evento
        chZero.clear();
        time.clear();
        chOne.clear();

    }

}

cout << "Gli eventi sono: " << iEv << endl;
```

```
    infile.close();

    return 0;
}
```

Bibliography

[1] A. Bettini, *Introduction to Elementary Particle Physics*, Cambridge University Press, 2014.

[2] Glenn F. Knoll, *Radiation Detection and Measurement*, John Wiley & Sons Inc., 2010.

[3] M. Tanabashi et al. (Particle Data Group), Phys. Rev. D 98, 030001 (2018).

[4] D.F. Measday, *The nuclear physics of muon capture*, Phys. Rept., 354, 243-409 (2011).

[5] Peter K.F. Greider, *cosmic rays at Earth*, Elsevier

[6] http://courses.washington.edu/phys433/muon_counting/statistics_tutorial.pdf